

Physiology and anatomy of synaptic connections between thick tufted pyramidal neurones in the developing rat neocortex

Henry Markram*, Joachim Lübke†, Michael Frotscher†, Arnd Roth and Bert Sakmann

*Max-Planck-Institut für Medizinische Forschung, Abteilung Zellphysiologie, Jahnstraße 29,
D-69120 Heidelberg and †Anatomisches Institut der Albert-Ludwigs-Universität Freiburg,
Albertstraße 17, D-79104 Freiburg, Germany*

1. Dual voltage recordings were made from pairs of adjacent, synaptically connected thick tufted layer 5 pyramidal neurones in brain slices of young rat (14–16 days) somatosensory cortex to examine the physiological properties of unitary EPSPs. Pre- and postsynaptic neurones were filled with biocytin and examined in the light and electron microscope to quantify the morphology of axonal and dendritic arbors and the number and location of synaptic contacts on the target neurone.
2. In 138 synaptic connections between pairs of pyramidal neurones 96 (70%) were unidirectional and 42 (30%) were bidirectional. The probability of finding a synaptic connection in dual recordings was 0·1. Unitary EPSPs evoked by a single presynaptic action potential (AP) had a mean peak amplitude ranging from 0·15 to 5·5 mV in different connections with a mean of $1\cdot3 \pm 1\cdot1$ mV, a latency of $1\cdot7 \pm 0\cdot9$ ms, a 20–80% rise time of $2\cdot9 \pm 2\cdot3$ ms and a decay time constant of 40 ± 18 ms at 32–34 °C and -60 ± 2 mV membrane potential.
3. Peak amplitudes of unitary EPSPs fluctuated randomly from trial to trial. The coefficient of variation (c.v.) of the unitary EPSP amplitudes ranged from 0·13 to 2·8 in different synaptic connections (mean, 0·52; median, 0·41). The percentage of failures of single APs to evoke a unitary EPSP ranged from 0 to 73% (mean, 14%; median, 7%). Both c.v. and percentage of failures decreased with increasing mean EPSP amplitude.
4. Postsynaptic glutamate receptors which mediate unitary EPSPs at -60 mV were predominantly of the L- α -amino-3-hydroxy-5-methyl-4-isoxazolepropionate (AMPA) receptor type. Receptors of the N-methyl-D-aspartate (NMDA) type contributed only a small fraction (< 20%) to the voltage-time integral of the unitary EPSP at -60 mV, but their contribution increased at more positive membrane potentials.
5. Branching patterns of dendrites and axon collaterals of forty-five synaptically connected neurones, when examined in the light microscope, indicated that the axonal and dendritic anatomy of both projecting and target neurones and of uni- and bidirectionally connected neurones was uniform.
6. The number of potential synaptic contacts formed by a presynaptic neurone on a target neurone varied between four and eight (mean, $5\cdot5 \pm 1\cdot1$ contacts; $n = 19$ connections). Synaptic contacts were preferentially located on basal dendrites (63%, 82 ± 35 μm from the soma, $n = 67$) and apical oblique dendrites (27%, 145 ± 59 μm , $n = 29$), and 35% of all contacts were located on tertiary basal dendritic branches. The mean geometric distances (from the soma) of the contacts of a connection varied between 80 and 585 μm (mean, 147 μm ; median, 105 μm). The correlation between EPSP amplitude and the number of morphologically determined synaptic contacts or the mean geometric distances from the soma was only weak (correlation coefficients were 0·2 and 0·26, respectively).
7. Compartmental models constructed from camera lucida drawings of eight target neurones showed that synaptic contacts were located at mean electrotonic distances between 0·07 and 0·33 from the soma (mean, 0·13). Simulations of unitary EPSPs, assuming quantal conductance changes with fast rise time and short duration, indicated that amplitudes of quantal EPSPs at the soma were attenuated, on average, to < 10% of dendritic EPSPs and varied in amplitude up to 10-fold depending on the dendritic location of synaptic contacts. The inferred quantal peak conductance increase varied between 1·5 and 5·5 nS (mean, 3 nS).
8. The combined physiological and morphological measurements in conjunction with EPSP simulations indicated that the 20-fold range in efficacy of the synaptic connections between thick tufted pyramidal neurones, which have their synaptic contacts preferentially located on basal and apical oblique dendrites, was due to differences in transmitter release probability of the projecting neurones and, to a lesser extent, to differences in the number of release sites per bouton or quantal size.
9. The continuum of efficacies in their synaptic connections implies that layer 5 pyramidal neurones can be recruited to ensemble electrical activity via their axon collaterals if as few as five of the strongly and reliably connected neighbouring neurones are active synchronously, whereas coincident APs of as many as 100 of the weakly connected pyramidal neurones are necessary.

* To whom correspondence should be addressed at the Department of Neurobiology,
The Weizmann Institute for Science, Rehovot, 76100 Israel.

Pyramidal neurones are output neurones of the neocortex (Ramón y Cajal, 1911; Valverde, 1986; for review see DeFelipe & Farinas, 1992). The neurones located in the superficial cortical layers (2/3) project to the contralateral hemisphere via the corpus callosum (Kasper, Lübke, Larkman & Blakemore, 1994b) while the deeper layer (5) neurones mainly project to subcortical targets (Wang & McCormick, 1993; Kasper *et al.* 1994b). The local axonal arborization of pyramidal neurones shows two distinct components: a more widespread, clustered horizontal arborization and vertical axonal collaterals. Horizontal axon collaterals establish synaptic contacts between neurones in the vicinity of cell bodies and also with neurones between cortical columns, while vertical axon collaterals establish connections between neurones of different layers within a column (Gilbert & Wiesel, 1979; Thomson & Deuchars, 1994).

To understand the functional circuitry within the cortex, it is necessary to establish the functional properties of synaptic connections linking neighbouring neurones within a layer as well as between different layers. Dual recordings from pairs of pyramidal neurones have made it possible to examine functional connectivity between pyramidal cells (Nicoll & Blakemore, 1990; Mason, Nicoll & Stratford, 1991; Thomson & West, 1993; Thomson, Deuchars & West, 1993; Deuchars, West & Thomson, 1994). However, pyramidal neurones in cortical layers constitute a heterogeneous population with distinct functional and anatomical properties (Connors & Gutnick, 1990). A dissection of the functional and anatomical connections between defined classes of neurones is therefore required to understand the cellular basis of the columnar organization of the neocortex and its division into functional maps.

In layer 5 of the visual cortex, two classes of pyramidal neurones have been described: the 'thick tufted' type, which tend to discharge bursts of action potentials (APs) and which project to the superior colliculus and pontine nuclei, and the 'slender untufted' type, which discharge more regularly and project to the cortex of the contralateral hemisphere via the corpus callosum (Chagnac-Amitai, Luhmann & Prince, 1990; Larkman & Mason, 1990; Mason & Larkman, 1990; Wang & McCormick, 1993; Kasper, Larkman, Lübke & Blakemore, 1994a). We examined the synaptic connections between pairs of thick tufted pyramidal neurones within layer 5 of rat somatosensory cortex to establish quantitatively their physiological and anatomical properties. The main purpose of the experiments was to determine how uniform these connections are anatomically and functionally and to understand how, on the one hand, anatomical factors such as the number and location of synaptic contacts and the dendritic arbor of a target neurone determine the efficacy of a synaptic connection and, on the other hand, how efficacy depends on functional factors like the mechanisms which underlie release of transmitter, size and time course of the postsynaptic conductance changes and dendritic voltage attenuation. For this purpose, infrared differential interference contrast (IR-DIC) microscopy was

employed to select thick tufted layer 5 pyramidal neurones in brain slices for dual whole-cell voltage recordings with patch pipettes. Filling both projecting and target neurones with biocytin made it possible to routinely examine both the physiological and morphological properties of their synaptic connections.

METHODS

Definition of terms used. The synaptic connection of a pair of neurones refers to all synaptic contacts formed on a target neurone by the collaterals of the axon of the projecting neurone. A single synaptic contact is made by a bouton, the synaptic cleft and the postsynaptic membrane.

Slice preparation. Wistar rats (14–16 days old) were decapitated and neocortical slices (sagittal; 300 µm thick) were cut on a vibratome (FTB, Bensheim, Germany) filled with iced extracellular solution (composition below). The right hemisphere was glued at the surface of the sagittal plane onto a block, which was mounted at an angle of 30 deg such that the blade cut from the upper border of the neocortex towards the caudal border and down towards the mid-line. Optimal slices (1–2 per hemisphere) for synaptically connected pairs were located approximately 3 mm from the lateral border of the neocortex. This slice orientation was found after examining slices with the aid of IR-DIC video-microscopy to visualize the morphology of the neurones, test recordings in each slice and labelling with biocytin to examine axonal and dendritic arbors. Slices were incubated for 30 min at 35 °C and then at room temperature (20–22 °C) until transferred to the recording chamber (32–34 °C). The extracellular solution contained (mm): 125 NaCl, 2.5 KCl, 25 glucose, 25 NaHCO₃, 1.25 NaH₂PO₄, 2 CaCl₂ and 1 MgCl₂. Layer 5 pyramidal neurones from the somatosensory cortical area were identified using IR-DIC microscopy with an upright microscope (Zeiss-Axioplan, fitted with a ×40-W/0.75 NA objective; Zeiss, Oberkochen, Germany) as previously described (Stuart, Dodt & Sakmann, 1993).

IR-DIC-guided selection of pairs of neurones. Slices were placed in the recording chamber such that the pial surface (dorsal) was up and anterior was left. Layer 5 pyramidal neurones were readily identified by their characteristically large somata, main apical dendrites and axon initial segment (Fig. 1). Pairs were selected according to their orientation within the slice relative to each other: (1) the main apical dendrites of the neurones were nearly parallel to the surface; (2) the axons were visible for at least 100 µm and (3) the apical dendrites and axons of both neurones were approximately parallel to each other. The pairs chosen were vertically and horizontally separated from each other by no more than 50 µm. They were located up to 120 µm below the surface of the slice, 80 µm on average.

Electrical recording. Somatic whole-cell recordings (6–12 MΩ pipette resistance, 10–25 MΩ access resistance as determined from the settings of the bridge balance in experiments where Axoclamp-2B amplifiers were used) were made and signals were amplified using an EPC-9 (List) in combination with either Axoclamp-2B (Axon Instruments) or EPC-7 amplifiers (List). Records were sampled at intervals of 10–400 µs and filtered at 3, 10 or 30 kHz using the program 'Pulse' (Heka Elektronik, Lambrecht, Germany), digitized by an ITC-16 interface (Instrutech, Great Neck, NY, USA) and stored on the hard disk of a Macintosh computer for off-line analysis (Igor Wavemetrics, Lake Oswego, OR, USA). Voltages were recorded with pipettes containing (mm): 100 potassium gluconate, 20 KCl, 4 ATP-Mg, 10 phosphocreatine, 0.3 GTP, 10 Hepes (pH 7.3, 310 mosmol l⁻¹, adjusted with sucrose),

and 50 U ml^{-1} creatine phosphokinase. In forty-five experiments 0·5% biocytin (Sigma) was added to the pipette solution and neurones were filled with biocytin by diffusion during 1–4 h of recording. Neurones typically had resting membrane potential (V_m) levels of $-60 \pm 2 \text{ mV}$. Membrane potentials were not corrected for the junction potentials between pipette and bath solution (between 7 and 8 mV). Input resistances were in the range of $50\text{--}120 \text{ M}\Omega$. To evoke a presynaptic AP, current pulses of 500 pA for 10 ms were used in most cases, and in about 20% of all cases 1 nA for 5 ms was used. Data are given as means \pm standard deviation (s.d.).

Analysis of electrical recordings. Whole-cell recording typically resulted in low-noise recordings. Noise is defined as the standard deviation of the amplitudes in a baseline interval of 50–100 ms recorded prior to the onset of the EPSP. Latency of EPSP onset was defined as the time from the peak of the AP to 5% of the EPSP amplitude. The sampling interval for about 70% of records was $400 \mu\text{s}$ ($10\text{--}200 \mu\text{s}$ in the remainder) and hence the time of the AP peak may not have been determined precisely. Furthermore, maximum capacitance compensation was also not made in all recordings, hence the AP may have been filtered and artificially ‘delayed’. The error estimated from recordings in which the sampling rate and capacitance compensation were adjusted appropriately was around $200 \mu\text{s}$. EPSP amplitudes were measured by averaging three to ten (depending on sampling rate) points around the peak. Amplitudes of the EPSP during trains of EPSPs were determined from exponential extrapolation of the decay of the preceding EPSP. Rise time was measured as the mean time to rise from 20 to 80% peak amplitude as determined from 20–300 individual sweeps without failures. The coefficient of variation (c.v.; standard deviation/mean) was corrected for baseline noise (variance of baseline noise was subtracted from the variance of the EPSP amplitude). As the EPSP amplitudes were obtained by averaging several data points, the c.v. was slightly underestimated by this procedure. The resulting relative error was, however, less than 1% on average. Failures were defined as events in which the amplitude in the selected interval was less than $1.6 \times$ noise (root mean square, r.m.s.) above the mean baseline level.

The decay time constant was measured from the average EPSP of 20–300 trials starting from a region where the EPSP had decayed to about 80% of the peak amplitude. While latency jitter may have caused some overestimation of decay time constants, this approach was more reliable than measuring the mean decay time constants of single sweeps since these measures were sensitive to spontaneous synaptic potentials. Only those synaptic connections in which all the parameters indicated in the Results section could be measured reliably were included in the summary of properties (138 connections). Additional experiments are also included in the connectivity ratio measurements since the recordings were sufficient to classify the connection as uni- or bidirectionally connected.

Pharmacological compounds. *N*-Methyl-D-aspartate receptors (NMDARs) were blocked using $50 \mu\text{M}$ D-(+)-2-amino-5-phosphonopentanoic acid (D-AP5; Tocris Neuramin, Bristol, UK), and L- α -amino-3-hydroxy-5-methyl-4-isoxazolepropionate receptors (AMPARs) were blocked using $10 \mu\text{M}$ 6-cyano-7-nitroquinoxaline-2,3-dione (CNQX; Tocris). Lidocaine (lignocaine), *N*-ethylbromide quaternary salt (QX-314, 5 mM; RBI, Bethesda, USA) was used to block voltage-gated channels. Calcium Green-1 was obtained from Molecular Probes.

Histological procedures. After recording, slices were fixed for 12–24 h in cold 100 mM phosphate-buffered solution (PB, pH 7·4) containing 1% paraformaldehyde and 1% glutaraldehyde. Thereafter, the slices were rinsed several times (10 min each) in PB.

To block endogenous peroxidases, slices were transferred into phosphate-buffered 3% H_2O_2 for 30 min. After washing in PB, sections were run through an ascending series of dimethyl sulphoxide (DMSO) at the following concentrations: 5, 10, 20 and 40%, diluted in 100 mM PB (30 min for each step). After five or six rinses in PB (10 min each) sections were incubated overnight at 4 °C in biotinylated horseradish peroxidase conjugated to avidin according to the manufacturer's protocol (ABC-Elite, Vector Labs, Peterborough, UK). Following incubation, sections were washed several times in PB and developed under visual control using a brightfield microscope (Zeiss Axioskop) until all processes of the cells appeared clearly visible (usually after 2–4 min). The reaction was stopped by transferring the sections into cold PB. After washing in the same buffer, slices were kept at 4 °C overnight in the same solution while shaking. To enhance the staining contrast, slices were postfixed for 1 h in 0·5% phosphate-buffered osmium tetroxide (Merck) and counterstained in 1% uranyl acetate. After several rinses in PB sections were flattened between a glass slide and a coverslip and dehydrated through an ascending series of ethanol in small glass vials. Following two 10 min washes in propylene oxide (Merck), slices were flat-embedded in Epon (Fluka, Hamburg, Germany) between coated glass slides. After polymerization, representative samples of well-filled pairs of neurones were photographed (Olympus BX-50) and drawn with a drawing tube using a $\times 40$ objective lens. These drawings formed the basis for the quantitative morphological analysis. Subsequent electron microscopy (EM) was carried out on five selected pairs of neurones. Serial sections were cut with an ultramicrotome (Leitz Ultracut, Leitz, Hamburg, Germany) and analysed for synaptic contacts using a Zeiss EM 10 electron microscope.

Quantitative morphological analysis. The following morphological parameters of synaptically connected thick tufted layer 5 pyramidal neurones were analysed quantitatively: (1) location of the soma within layer 5, (2) soma diameter (vertical and horizontal), (3) number and maximum span of dendritic fields of basal, apical oblique, and terminal tuft dendrites, (4) distances from the soma to the first bifurcation of the apical dendrite, and (5) number and maximum extent of horizontal and vertical axonal collaterals. Furthermore, the number of potential synaptic contacts established by the two neurones and the distances of the synapses from the perikarya were determined for the main apical trunk, basal and apical oblique dendrites of different orders, and for the terminal tuft. Potential synaptic contacts were identified as close apposition of a bouton and dendrite in the same focal plane (see Fig. 11*B*–*D*). For all data the means \pm s.d. were calculated.

Construction of geometric and electrical models of pyramidal neurones. Compartmental models were constructed from camera lucida drawings of pairs of pyramidal neurones. The lengths and diameters of all dendritic branches were measured from enlargements of these camera lucida drawings, tabulated and entered in the program package NEURON (Hines, 1993). Geometric and electrotonic dendrograms were constructed from these tabulated values using a program written in Mathematica (Wolfram Research, Champaign, IL, USA; see Fig. 20 legend). All simulations were done on a Sun Sparcstation 2 (Sun Microsystems, Mountain View, CA, USA). The values for passive cable properties were assumed as $R_i = 155 \Omega \text{ cm}$, $C_m = 1 \mu\text{F cm}^{-2}$ and $R_m = 70000 \Omega \text{ cm}^2$ (where R_i is the internal resistivity, C_m is the membrane capacitance and R_m is the membrane resistance) similar to the values reported by Spruston & Johnston (1992). The passive reversal potential was set to -70 mV . The spine area was assumed to be 50% of the total dendritic surface area. Axon collaterals were not included in the compartmental models. The hyperpolarization-activated current

(I_h) is one of the factors which determine the shape of the EPSP and was included in most simulations. It was modelled as two simultaneous first-order processes (Spain, Schwindt & Crill, 1987) with time constants of activation of 75 and 319 ms and relative amplitudes of 0.8 and 0.2 for the fast and slow processes, respectively. The reversal potential was -32 mV, half-maximum activation was at -82 mV, and the slope factor in the Boltzmann equation describing equilibrium activation was 7 mV. The density of channels underlying I_h was assumed to be homogeneous, with a maximum conductivity of $123.76 \mu\text{S cm}^{-2}$, which was chosen in order to achieve a resting membrane potential of -60 mV. Including I_h in the simulations affected predominantly the decay time course of the EPSP.

Simulation of quantal conductance change at single synaptic contacts. To simulate dendritic attenuation of EPSPs, the time course of a quantal conductance change mediated by AMPARs at single synaptic contacts was described by the sum of two exponentials. The time constants were 0.2 and 1.5 ms for the rising and decay phases, respectively, and the 'standard' peak conductance was 2.7 nS, a typical value determined from simulations of unitary EPSPs in eight reconstructed connections (see below). The number of AMPAR channels open at the peak of a quantal conductance change would be 225 assuming a single-channel conductance of 12 pS. Synaptic contacts were placed at the head of explicitly modelled spines. Spine neck length was 1 μm , neck diameter was 0.35 μm and head length and diameter were both 0.7 μm (Peters & Kaiserman-Abramof, 1970). Their series resistance was 19 M Ω . The quantal conductance change mediated by NMDAR channels was modelled similarly; the peak conductance change was 5.4 pS at a membrane potential of -60 mV in the presence of 1 mM extracellular Mg²⁺, with a rise time constant of 4.6 ms and a decay time constant of 39 ms (derived assuming that a Q_{10} of 3 applies to the values of Monyer *et al.* 1992, for the NR1-NR2A channel type). The current-voltage ($I-V$) relations for NR1-NR2A in the absence and presence of extracellular Mg²⁺ were given as 4th-order polynomials (Burnashev, Zhou, Neher & Sakmann, 1995). These conductance changes were used as input functions for the compartmental model at the identified synaptic contacts to simulate EPSPs.

Simulation of unitary EPSPs. To measure the variability of unitary EPSP amplitudes caused by differences in dendritic location of contacts and to obtain an estimate of the peak quantal conductance change, unitary EPSPs were simulated. In the binomial model of transmitter release, the unitary EPSP amplitude is given by $\Delta V = n_b p_r q_s$, where n_b is the number of release sites, p_r is the release probability and q_s is the quantal EPSP amplitude at the soma. To obtain the conductance change, g_q , underlying q_s , unitary EPSPs were simulated in connections with a known number of synaptic contacts (n_a) and their dendritic location using the compartmental models and conductance transients described above. The assumption was made that each synaptic contact has only one active release site ($n_b = n_a$). The anatomical correlate of a release site would be an active zone.

In a first approximation, p_r was estimated from the measured (noise corrected) coefficient of variation (c.v.) according to $p_r = 1/(1 + n_b(\text{c.v.})^2)$. Then, p_r was corrected further taking into account the contribution to variability caused by the differences in distances of the synaptic contacts from the soma. The coefficient of variation, $(\text{c.v.})_q$, of the somatic amplitude of simulated standard quantal EPSPs, generated at different synaptic contacts in a given connection, was computed. For each of the eight connections, it was included in the expression for the release probability as (see Appendix):

$$p_r = \frac{1 + (\text{c.v.})_q^2}{1 + (\text{c.v.})_q^2 + n_b(\text{c.v.})^2}. \quad (1)$$

The amplitude, g_q , and kinetics of the simulated quantal conductance were similar to the ones used for the simulation of quantal EPSPs. To include channel-gating noise, 300 simulated traces of the synaptic conductance at a single contact were obtained by Monte Carlo simulation of glutamate diffusion in the synaptic cleft coupled to AMPA receptor gating (Bartol, Land, Salpeter & Salpeter, 1991) using a program written in C by A. Roth. These simulations made use of a kinetic model for AMPARs in somatic patches from hippocampal CA3 pyramidal neurones given in Jonas, Major & Sakmann (1993). The rate constants were modified in order to reproduce the slower recovery from desensitization found in

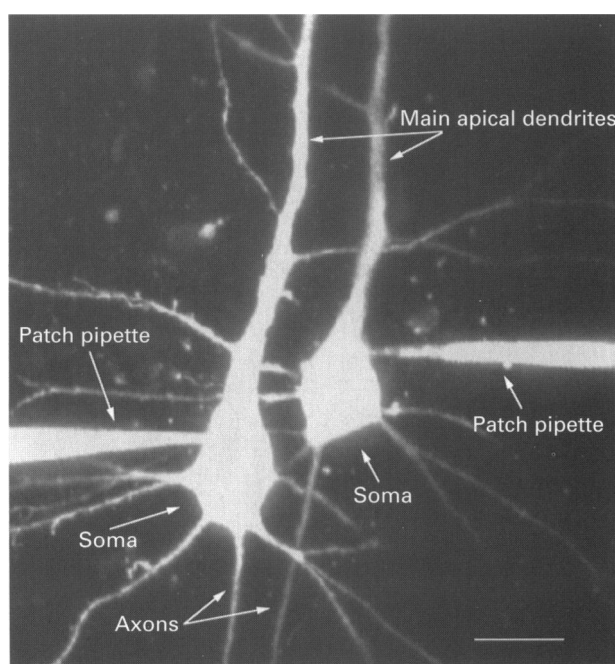


Figure 1. Dual whole-cell recording from layer 5 pyramidal neurones

Confocal maximal intensity reconstruction (stack of 30 images, 1 μm depth increments) of a pair of adjacent, synaptically connected layer 5 pyramidal neurones that were identified using IR-DIC microscopy and recorded with patch pipettes. Neurones were loaded with a calcium-sensitive fluorescent indicator, Calcium Green-1 (100 μM). Scale bar, 20 μm .

layer 5 pyramidal neurones (Jonas, Racca, Sakmann, Seeburg & Monyer, 1994). To account for the higher temperature ($32\text{--}34^\circ\text{C}$), all rate constants in this model were increased by a factor of 1.7. The diffusion coefficient of glutamate in the synaptic cleft was assumed to be $3 \times 10^{-6} \text{ cm}^2 \text{ s}^{-1}$, the cleft was assumed to be cylindrical with a height of 20 nm and a diameter of 1 μm , and the number of glutamate molecules per vesicle was assumed to be 5000 (Jonas, Major & Sakmann, 1993). Due to the long run-time of the Monte Carlo simulations it was not practical to calculate matched numbers of available AMPA receptors reproducing the average EPSP amplitudes (ΔV) measured in every target cell. Instead, the synaptic conductances obtained with the standard number of available AMPA receptors (550) were multiplied by a constant factor varying between 0.49 and 1.86 (mean, 1.03; s.d., 0.5). Both the release probability, p_r , and peak conductance, g_0 , were assumed to be the same for all synaptic contacts of a particular connection.

For each connection 450 unitary EPSPs were simulated by randomly activating a synaptic conductance at each contact with probability p_r . Each time a synaptic conductance function was selected at random from the set of 300 simulated synaptic conductance functions and shifted in time according to axonal delay and latency of release. The axonal AP conduction velocity was assumed to be 0.3 m s^{-1} . The latency distribution of quantal release was taken from Borst & Sakmann (1996). When corrected for the higher temperature ($Q_{10} = 3$), it had a mean of $0.47 \pm 0.12 \text{ ms}$ ($\pm \text{s.d.}$). The dendritic delay is measured as the time interval between the beginning of the synaptic conductance increase and the onset of the somatic EPSP (5% of the peak amplitude).

Frequency-dependent EPSP depression. A graphical c.v. analysis (Faber & Korn, 1991) was used to estimate the possible contribution of pre- and postsynaptic mechanisms to the reduction of unitary EPSP amplitudes during frequency-dependent depression. The ratio $(\text{c.v.})_i^2 / (\text{c.v.})_1^2$ was plotted against $\Delta V_i / \Delta V_1$ for the first five unitary EPSPs and the linear regression line was measured. $(\text{c.v.})_i$ and ΔV_i refer to the first EPSP in the train and $(\text{c.v.})_i$ and ΔV_i refer to the i th EPSP in the train.

Shortcomings of morphological reconstructions. Simulations are subject to several inaccuracies. Most notably, the camera lucida drawing was a projection of the morphology of the neurone onto a plane. Corrections for the z -direction perpendicular to the plane were not taken into account. This is unlikely to be a problem for the estimation of the lengths of the apical dendrites, as they were reasonably parallel to the plane of projection. However, basal dendrites, obliques and especially the apical tuft branches may appear too short in the reconstruction. Both geometric and electrotonic lengths may have been underestimated by 20%, on average.

Tissue shrinkage due to the fixation procedure was not compensated for. The shrinkage of the tissue surrounding the biocytin-stained cells is expected to be about 10–20%. The size of the wiggles seen in the apical dendrites suggests that the reconstructed cells experienced about 10% less shrinkage than their environment, probably because they were stabilized by the reaction product. Therefore, the shrinkage of the biocytin-filled cells is estimated to be around 5%, which is consistent with the results of a comparison of soma diameters measured in the IR-DIC image and the camera lucida drawing of the same cells.

There is also some uncertainty about the values of the passive cable properties and the parameters in the model for I_h . Specifically, the assumption of homogeneity of these parameters may not be valid.

RESULTS

Physiology of synaptic transmission between layer 5 pyramidal neurones

Identification of synaptically connected pairs of pyramidal neurones. IR-DIC microscopy facilitated the selection of pairs of neurones according to morphological criteria. Adjacent thick tufted layer 5 pyramidal neurones (Fig. 1) with soma sizes between 15 and 25 μm (vertical

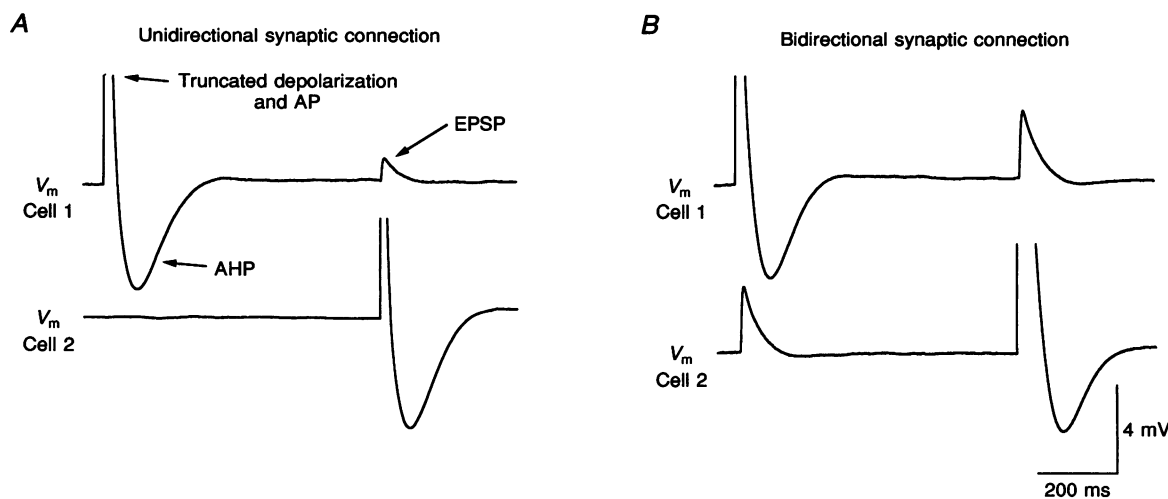


Figure 2. Uni- and bidirectional synaptic connections between pairs of pyramidal neurones

Simultaneous voltage recordings from two synaptically connected neurones. Each trace represents the average of 75 records. *A*, unidirectionally connected pair of neurones. Single AP evoked in cell 1 fails to elicit an EPSP in cell 2 while a single AP in cell 2 elicits a unitary EPSP in cell 1. *B*, bidirectionally connected pair of neurones. Single AP in either cell 1 or cell 2 elicits unitary EPSP in the other cell. V_m , membrane potential.

diameter) were selected for recording according to the criteria outlined in Methods.

The probability of finding a synaptic connection between two simultaneously recorded pyramidal neurones was 0.1 as determined from a sample of 500 paired recordings. It is, however, not clear how accurately this value reflects the ratio of connections between neighbouring neurones since the probability of obtaining records from connected pairs of neurones varied from one slice preparation to another and increased during the course of all experiments. In one brain slice, for example, in which successive dual recordings from six pairs of neurones were made, two pairs were coupled bidirectionally, three were unidirectionally coupled and one pair was not connected, suggesting that the probability of connections between two neurones may be considerably higher than the overall value of 0.1. Moreover, some axon collaterals were cut during the preparation of the brain slices.

Whole-cell voltage recording combined with signal averaging reliably revealed the presence of a synaptic connection. After dual whole-cell voltage recording was

established, single presynaptic action potentials (APs) were evoked in either neurone. Recordings from 138 synaptic connections were obtained, of which 96 (70%) were unidirectionally coupled (Fig. 2A) and 42 (30%) were connected bidirectionally (Fig. 2B). This percentage is higher than expected and could indicate that the actual connection ratio is higher than 0.1 or that there was a sampling bias. Stimulation by a single AP (at least 10–20 trials) may have resulted in the exclusion of some synaptic connections that have a high percentage of failures (above 60%). The physiological properties of EPSPs in uni- and bidirectional connections were almost indistinguishable and the results were therefore pooled (see below).

Latency, time course and amplitude of unitary EPSPs. Figure 3A illustrates at higher resolution the time course of APs evoked in the soma of a presynaptic neurone by current injection (upper trace), which elicited unitary excitatory postsynaptic potentials (unitary EPSPs) in the target neurone (lower traces) with a delay in the range of milliseconds and which had variable amplitudes and

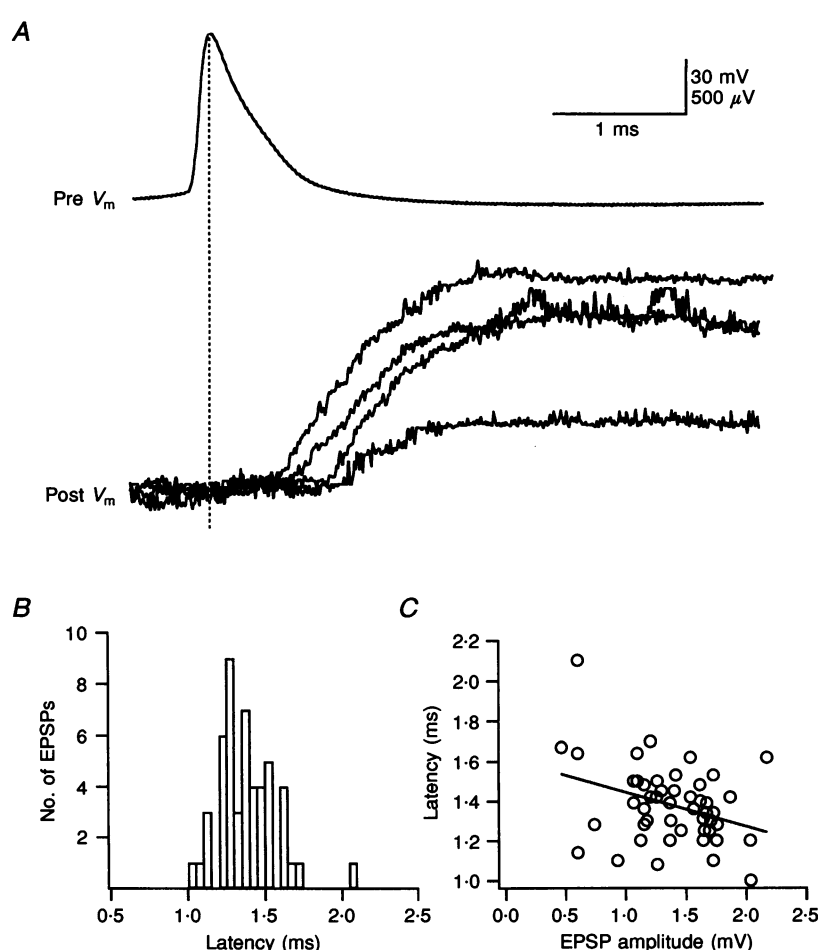


Figure 3. Latency fluctuations of single unitary EPSPs

A, record of presynaptic AP (upper trace) and unitary EPSPs (lower traces) showing fluctuation in synaptic latency measured between the peak of AP and beginning of EPSP. B, distribution of latencies of unitary EPSPs. C, plot of latency against peak EPSP amplitude showing inverse relationship. Correlation coefficient is -0.34 and slope is -0.17 ms mV^{-1} for this experiment.

latencies upon successive APs. The latency of the unitary EPSP, measured as the time interval from the peak of the presynaptic AP to the onset of the EPSP (5% of peak amplitude), fluctuated from trial to trial in individual synaptic connections up to 4-fold (as measured in three connections). Latency histograms were singly peaked (Fig. 3B) and there was a weak negative correlation of latency with EPSP amplitude (Fig. 3C).

The mean latency, measured in 138 connections was 1.7 ± 0.9 ms (Fig. 4A and C) and decreased with EPSP size (slope, -0.14 ms mV $^{-1}$; correlation coefficient, -0.17). The mean 20–80% amplitude rise time, measured as indicated in Fig. 4A (arrows) was 2.9 ± 2.3 ms (Fig. 4D) and EPSPs had a mean peak amplitude of 1.3 ± 1.1 mV (Fig. 4E). The decay time course of unitary EPSPs could be fitted in most experiments by a single exponential (Fig. 4B) with a decay

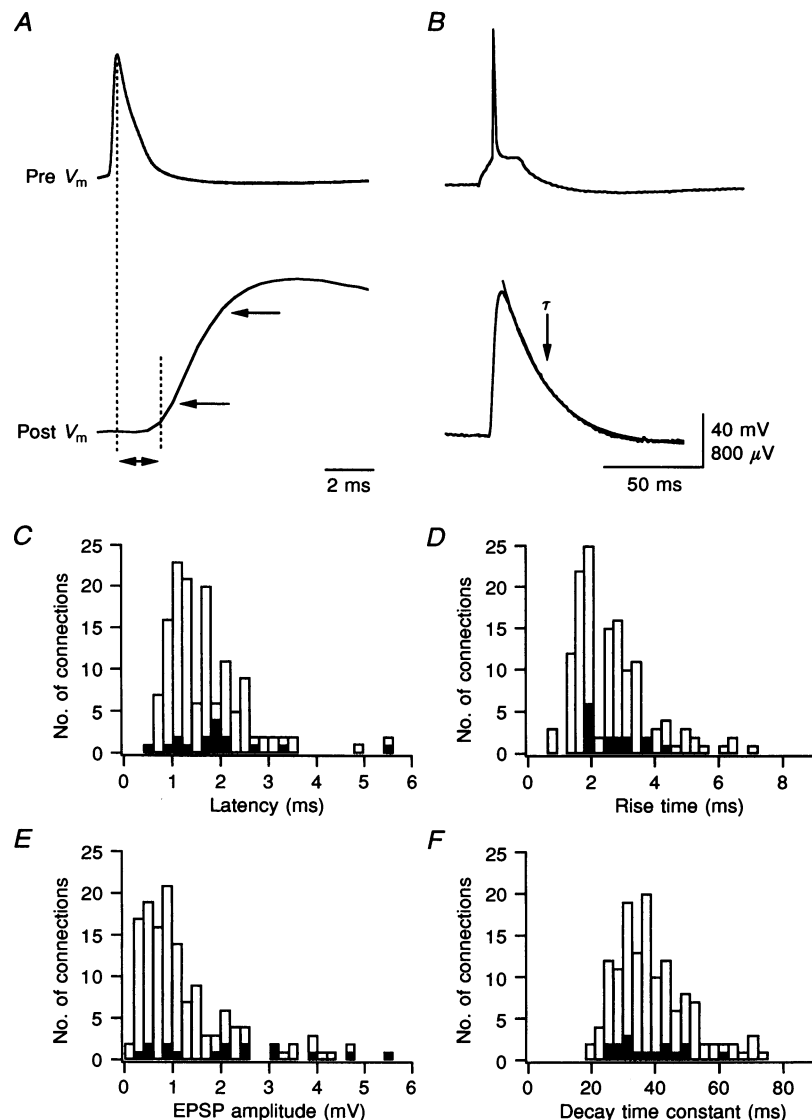


Figure 4. Average time course and amplitude of unitary EPSPs

A and B illustrate the rise and decay time course of mean unitary EPSPs (lower traces) evoked by APs shown in upper traces. EPSP traces represent averages of 20 unitary EPSPs. Dashed lines in A represent mean latency (AP peak to 5% of the EPSP peak amplitude), arrows point to 20 and 80% peak amplitude, respectively. Single-exponential fit is superimposed on the decay of the mean EPSP in B (smooth curve). Scale bar refers to upper (40 mV) and lower (800 μ V) voltage traces. C, histogram of latencies of EPSP onset, measured from the peak of the presynaptic AP to 5% of the rise of the EPSP as detailed in A (mean, 1.7 ms; median, 1.5 ms). D, histogram of 20–80% peak amplitude rise times (mean, 2.93 ms; median, 2.4 ms). E, histogram of peak amplitudes (mean, 1.28 mV; median, 0.98 mV). F, histogram of mean decay time constants at -60 ± 2 mV membrane potential (mean, 40.2 ms; median, 37 ms). All histograms were from the 138 synaptic connections. The filled bars represent results from a subset of 16 connections which were analysed morphologically. In 3 of the 19 anatomically reconstructed connections not all EPSP parameters shown in this figure could be measured.

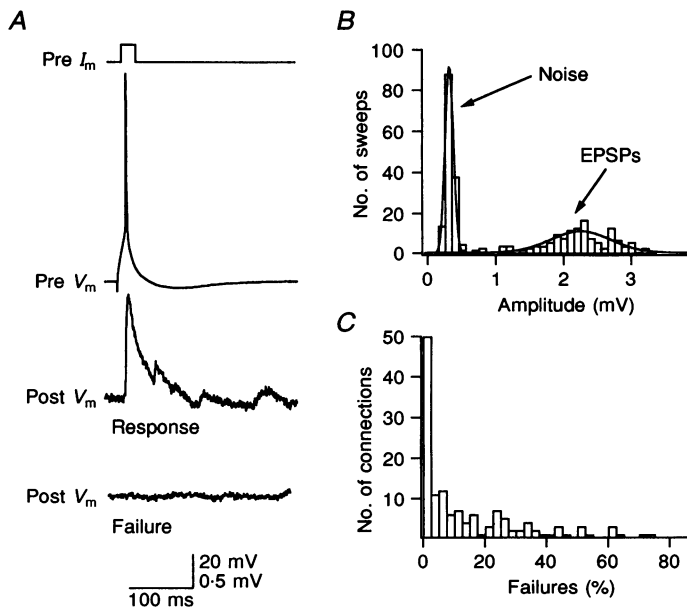


Figure 5. Reliability of synaptic transmission

A, example of success and failure of a single presynaptic AP (upper trace) to elicit a unitary EPSP. Failure is defined as an event in which the amplitude was below the limit of $1.6 \times$ noise (r.m.s.). A single response and a failure are shown in middle and lower trace. I_m shows the time course of current injected via the recording pipette. *B*, histogram of background noise and amplitudes of the EPSPs for 150 sweeps. *C*, histogram of percentage of failures (mean, 14.3%; median, 6.5%). Percentage of failures was determined from 30–150 trials in each connection.

time constant of 40 ± 18 ms (Fig. 4*F*). Latency, rise time and decay time constants of uni- and bidirectionally coupled neurones were not significantly different ($P > 0.2$, two-tailed Student's *t* test). Mean peak EPSP amplitudes of the same sample were slightly different (1.16 ± 0.96 and 1.57 ± 1.25 mV; $P = 0.037$).

Reliability of horizontal synaptic connections. In the majority of experiments, the low background noise (0.08 – 0.51 mV (r.m.s.); mean, 0.23 ± 0.07 mV; $n = 138$) of whole-cell voltage recording permitted unequivocal detection of responses or of failure of a presynaptic AP to evoke an EPSP (Fig. 5*A* and *B*). On average, synaptic connections between pyramidal neurones transmit reliably since the

mean percentage of failures was only $14.3 \pm 17.6\%$, while the median was 6.5% (Fig. 5*C*). Despite the relatively low failure rate, the peak amplitudes of unitary EPSPs fluctuated randomly from trial to trial around a mean value (Fig. 6*A*–*C*) with a c.v. ranging between 0.13 and 2.8 in different experiments (mean, 0.52 ± 0.37 ; Fig. 6*D*).

Many of the distributions were non-Gaussian as judged by the skewness, S , of the distribution:

$$S = \frac{1}{N} \sum_{i=1}^N (\Delta V_i - \bar{\Delta} V)^3,$$

where ΔV_i is the peak amplitude of the i th sweep, $\bar{\Delta} V$ is the mean peak amplitude and N is the number of sweeps. The cubic root of the skewness ranged as follows: $-0.51 \text{ mV} \leq \sqrt[3]{S} \leq +0.2 \text{ mV}$ in

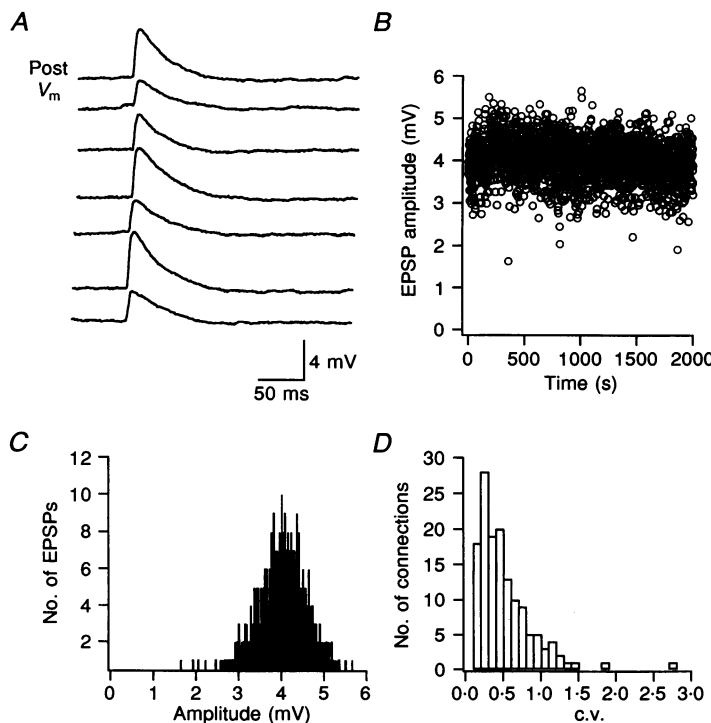


Figure 6. Fluctuation of unitary EPSP amplitude

A, examples of successive unitary EPSPs recorded every 4 s from one connection. *B*, peak amplitudes of unitary EPSPs as a function of time. Failures were not observed. Same connection as in *A*. *C*, histogram of EPSP peak amplitudes. For this connection the c.v. was very small (0.15). Same connection as in *A*. *D*, distribution of c.v.s of 140 synaptic connections (mean, 0.52; median, 0.41).

different experiments. Given in relation to the mean peak amplitude ΔV , it was $-0.5 \leq \sqrt{S}/\Delta V \leq +0.7$, being positive for EPSPs when the calculated release probability (see below) was <0.5 .

Figure 7 illustrates the large range of both the rate of failures (Fig. 7A) and the c.v. (Fig. 7B) observed in 140 different synaptic connections. Failure rate and c.v. decreased with increasing EPSP amplitude. In a binomial model of synaptic transmission, this shape of the relation is expected if the release probability is a main determinant of the unitary EPSP amplitude.

Attempts to fit a binomial model to these data (minimizing squared deviation) where $c.v. = \sqrt{[(1 - p_r)/(n_b p_r)]}$ and $p_r = \Delta V/(n_b q_s)$ with a single set of values for the number of release sites (n_b) and the quantal EPSP size at the soma (q_s) were unsatisfactory because the best fit excluded all data points for EPSPs larger than 2.5 mV. To delineate limits of p_r and q_s , it was assumed that n_b is equal to 6, as this is about the mean number of synaptic contacts found in anatomical reconstructions (open circles and squares). The two limiting curves shown in Fig. 7 were calculated for $q_s = 0.2$ and 1.0 mV and enclose almost all data points, suggesting that p_r may vary over an almost 40-fold range (0.025–0.9) in these 140 connections (Fig. 7 legend), whereas q_s varied over a 5-fold range. An alternative interpretation could be that the number of release sites per anatomically identified synaptic contact (n_b/n_a) was larger in connections with larger mean EPSP amplitudes (Fig. 7A and B, dotted lines).

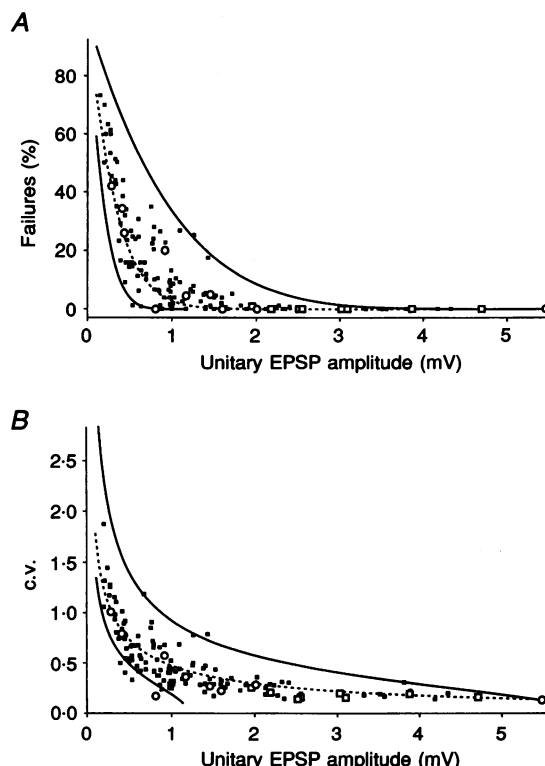
Voltage dependence of unitary EPSPs. Unitary EPSPs had a characteristic voltage dependence consistent with that described by Thomson & West (1993), where the peak

amplitude, the decay time constant and the voltage integral increased upon depolarization of the membrane potential of the postsynaptic neurone to values more positive than -60 mV, facilitating the initiation of an AP at -50 mV or more positive (Fig. 8A–C). This amplification of unitary EPSPs may be caused by several mechanisms, including increased current through NMDAR channels, block of I_h channels and activation of low-threshold Ca^{2+} or non-inactivating somatic Na^+ channels (Stafstrom, Schwindt & Crill, 1982; Deisz, Fortin & Ziegler, 1991; Nicoll, Larkman & Blakemore, 1993; Markram & Sakmann, 1994; Stuart & Sakmann, 1995).

AMPARs and NMDARs mediate unitary EPSPs. The contribution of AMPAR and NMDAR channels to EPSPs was examined by the pharmacological blocking of either class of glutamate receptors. Bath application of 10 μM CNQX, an antagonist of AMPAR channels, blocked EPSPs at -60 mV almost completely (about 95% reduction in peak amplitude), indicating that at this potential they are mediated predominantly by AMPAR channels. The time course of the remaining unitary EPSP mediated by NMDAR channels could not, however, be resolved quantitatively ($n = 7$, not shown). To examine the contribution of NMDAR channels more directly, D-AP5 (50 μM), an antagonist of NMDARs, was added to the bath solution and the difference in EPSP peak amplitude and its voltage–time integral before and during D-AP5 application was measured. The postsynaptic neurone was first loaded with QX-314 (5 mM) to block EPSP amplification by voltage-activated channels and unitary EPSPs were measured at different membrane potentials. At -80 mV, a difference between the unitary EPSPs was not detectable (Fig. 9A, C and D) whereas at

Figure 7. Decrease of failures and c.v. with increasing EPSP amplitude

A, percentage of failures is plotted as a function of EPSP size for 140 connections. Open circles are from 10 connections with a known number of contacts and geometric distance from the soma. Open squares are for 8 connections with completely reconstructed morphology, for which the number of synaptic contacts and geometric and calculated electrotonic distances from the soma are known. The two continuous lines represent the prediction of binomial release statistics for the percentage of failures as a function of EPSP amplitude with $n_b = 6$ and $q_s = 0.2$ mV (left) and $q_s = 1$ mV (right) as the p_r values increase from 0.125 to 0.9 (left) and from 0.025 to 0.9 (right). These p_r values refer to the two end-points of each curve. The dotted line represents the predicted values calculated when the assumption is made that the number of synaptic contacts, n_a , is 6 and that the number of release sites per synaptic contact, n_b/n_a , increases linearly from 1 to 4 as the EPSP amplitude increases from zero to 5.5 mV. B, coefficient of variation is plotted as a function of mean peak EPSP amplitude. Lower and upper continuous lines and the dotted line have the same parameters as the continuous and dotted lines in A.



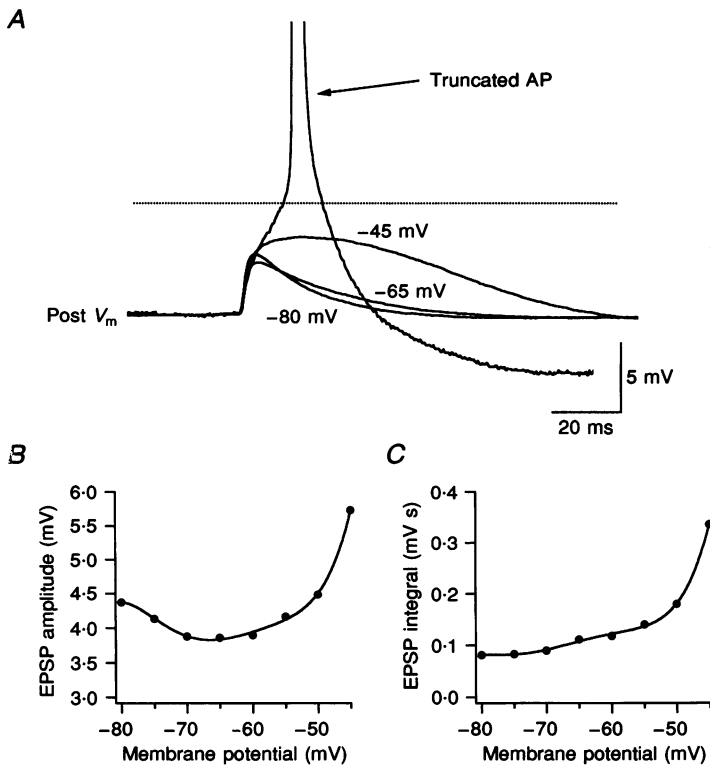


Figure 8. Voltage dependence of unitary EPSPs

A, unitary EPSPs at different holding membrane potentials (each trace is a mean of 30 individual unitary EPSPs). A single response where the unitary EPSP initiated a postsynaptic AP (from -45 mV membrane potential) is also superimposed. The baseline at different membrane potentials was vertically aligned. The dotted horizontal line indicates the threshold for AP initiation by an EPSP when the soma was depolarized to -45 mV . Voltage dependence of the EPSP amplitudes and integrals is shown below in B and C. Data points in B and C were connected by fitting to 5th-order polynomials.

-30 mV , both peak amplitude and the voltage–time integral were substantially reduced (Fig. 9B–D). The component blocked by d-AP5 probably reflects the contribution of NMDAR channels. The block was reversed completely after 20 min superfusion of the slice with normal external solution ($n = 3$; not shown).

Depression and facilitation of unitary EPSPs during bursts of presynaptic APs. Synaptic transmission between pyramidal neurones via the horizontal connections during trains of presynaptic APs was examined because *in vivo* layer 5 thick tufted pyramidal neurones are

characterized by burst-like electrical activity (Connors & Gutnick, 1990). Unitary EPSP peak amplitudes decayed rapidly to $< 50\%$ of the amplitude of the first EPSP when evoked by a train of presynaptic APs ($\geq 5\text{ Hz}$ frequency) in all connections examined ($n = 15$). The largest amplitude reduction occurred during the initial two to four EPSPs and was accompanied by an increase in the c.v. of the peak amplitudes of successive EPSPs.

A coefficient of variation analysis of peak EPSP amplitudes, assuming binomial release statistics (Faber & Korn, 1991), was made for five connections where EPSPs were evoked by trains

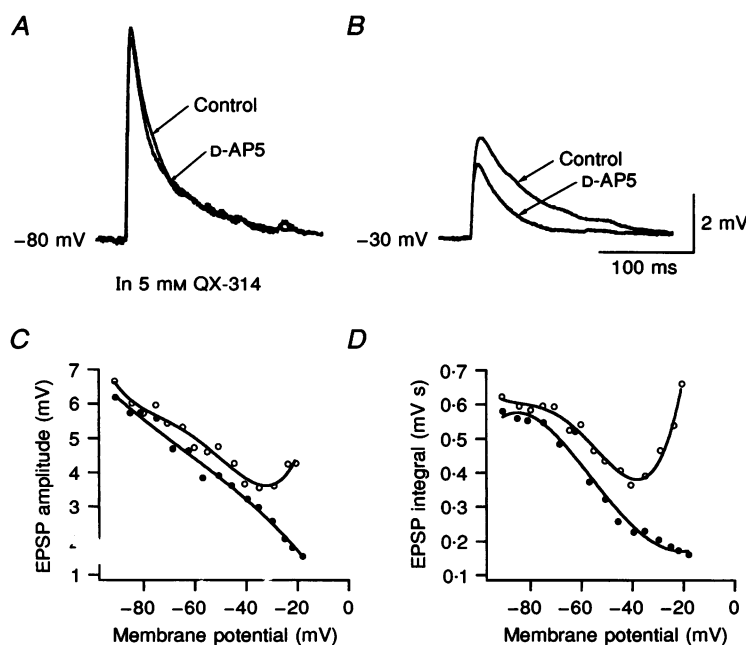


Figure 9. AMPAR and NMDAR components of unitary EPSPs

Control neurones were loaded with QX-314 (5 mM) to block voltage-activated Na^+ channels and control unitary EPSPs were recorded at different holding potentials. d-AP5 was bath applied and EPSPs were recorded again at different potentials. A, unitary EPSPs before and during d-AP5 application at -80 mV . B, at -30 mV . C, voltage dependence of the EPSP peak amplitude before and during d-AP5. D, voltage dependence of EPSP voltage integral. At -80 mV , the difference in voltage integral before and during d-AP5 was insignificant; at -60 mV it was 17% and at -50 mV it was 26% in this experiment and $31 \pm 7\%$ ($n = 6$) on average. At -30 mV , it was 55%. Data points in C and D were fitted with 5th-order polynomials. Open circle, control; filled circle, d-AP5.

(5 Hz) of presynaptic APs. The inverse of their squared c.v.s plotted for the first five normalized unitary EPSPs indicated that both pre- and postsynaptic mechanisms may underlie reduction of the EPSP amplitudes, as the linear regression line has a slope > 0 and < 1 .

The degree of EPSP amplitude depression was frequency dependent. Depression became measurable when presynaptic APs were elicited at 1 AP s $^{-1}$ or more frequently, and amplitudes of the initial two to four EPSPs following the first EPSP in a train decreased more rapidly as the frequency of presynaptic APs increased. The strong amplitude reduction of unitary EPSPs during a train of presynaptic APs indicates that, in these connections, paired-pulse facilitation or frequency-dependent short-term facilitation seen in other CNS synapses is not regularly observed. This does not, however, imply that facilitation could not occur because in some connections frequency-dependent facilitation was observed when $[Ca^{2+}]_o$ was lowered from 2 to 1 mM ($n = 3$). In most other connections ($n > 10$), however, depression was still present even at 1 mM $[Ca^{2+}]_o$. Therefore, frequency-dependent facilitation appears to be masked by concomitant frequency-dependent depression.

Morphology of synaptically connected layer 5 pyramidal neurones

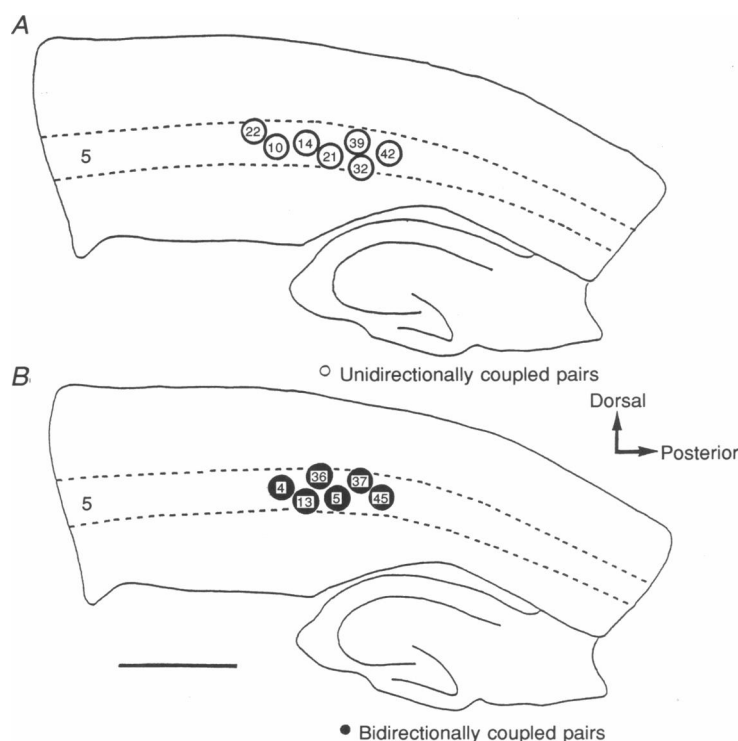
Figure 10 illustrates the location in the somatosensory cortex of thirteen anatomically reconstructed pairs of synaptically connected neurones (26 neurones). The locations of thirty-two reconstructed pairs in another sample, which were only partially analysed, were distributed similarly (not shown). This indicates that the dual whole-cell voltage recordings were obtained exclusively from neurones within layer 5 of the somatosensory cortex.

Unidirectional synaptic connections. Seven pairs of unidirectionally connected neurones were reconstructed and analysed in detail with respect to the dendritic location of the synaptic contacts made on the target neurone by the presynaptic neurone. Figure 11 illustrates a pair of connected neurones at low magnification after filling with biocytin (Fig. 11A) and potential synaptic contacts at different dendritic locations at higher magnification (Fig. 11B–D). Both neurones were reconstructed with the aid of a camera lucida, and potential synaptic sites on the target neurone were marked on the camera lucida reconstructions (Fig. 12). Morphological features of projecting and target neurones, such as the size of the cell body and the pattern of dendritic and axonal arborization are quantified in Table 1. Statistical significance for different dendritic and axonal parameters was tested for each pair of projecting and target neurones using the Wilcoxon signed-rank test. The test confirmed that this sample of neurones constituted a homogeneous class (significance level, $\alpha = 0.05$).

Potential synaptic contacts were found exclusively on dendrites. Typically, five or more contacts were established with the target neurone (5.6 ± 1.1 ; minimum, 5; maximum, 8), and these contacts were found on the entire dendritic tree. Despite this distributed innervation, synaptic contacts tended to be located at specific dendritic locations. Of all potential synaptic contacts identified, 58% were located on basal dendrites. Of these, 91% were located on secondary and tertiary dendritic branches at a distance of 60–100 μm from the soma (Table 3). In one connection, however, three contacts were located on the terminal tuft branches of the target neurone in layer 1 (Fig. 13).

Figure 10. Location of synaptically connected and morphologically reconstructed pairs of thick tufted layer 5 neurones

A and *B*, schematic drawings of two sections. Location of the reconstructed unidirectionally (*A*) and bidirectionally (*B*) connected pairs of neurones is indicated by circles. Numbers within circles denote internal reference numbers. The borders of layer 5 are marked by dashed lines. All neurones were located within the somatosensory cortex. Scale bar, 1 mm.



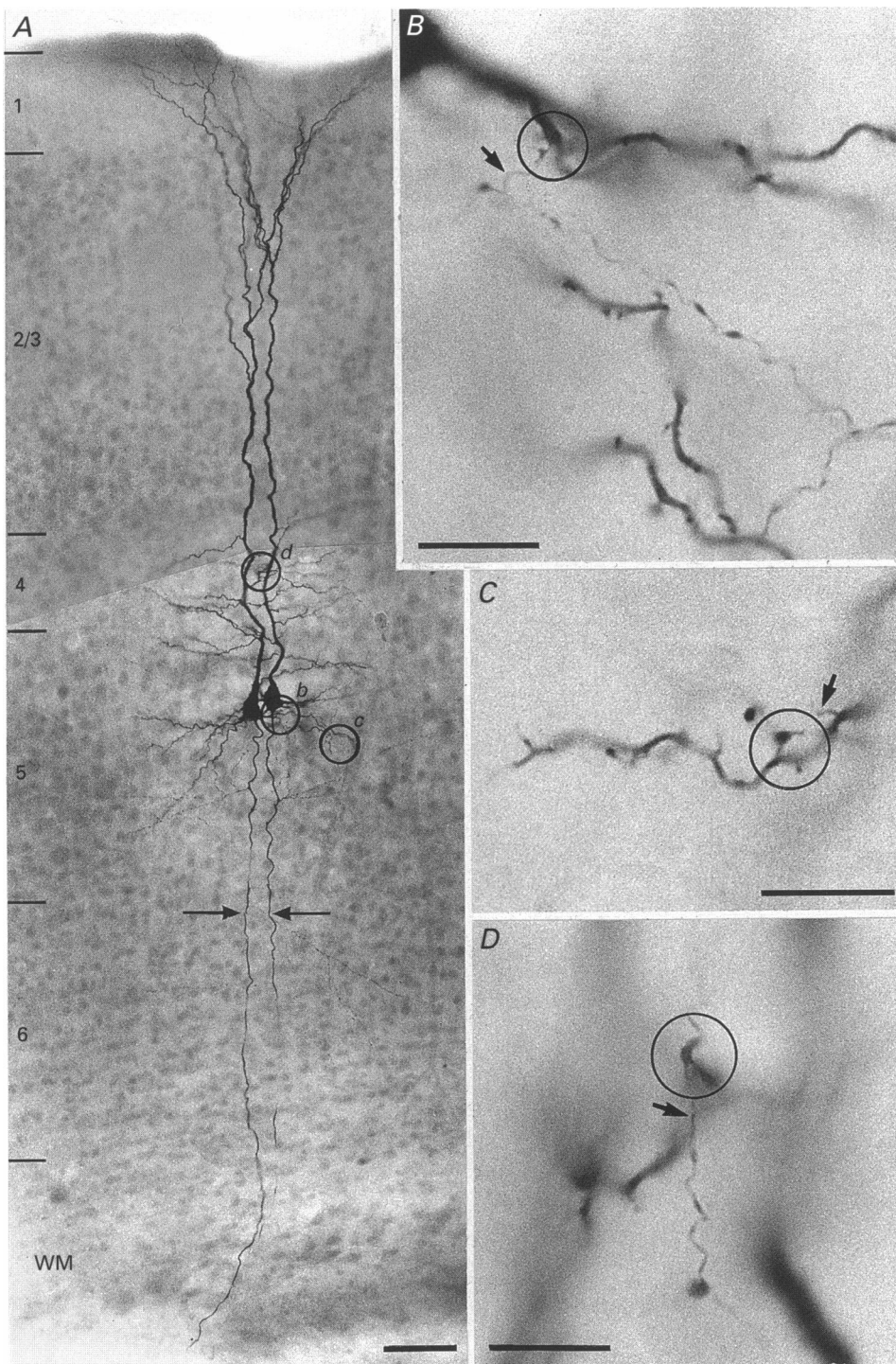


Figure 11. Unidirectionally connected pair of thick tufted layer 5 pyramidal neurones

A, low magnification of a light microscopic image of a connected pair of neurones filled with biocytin. Open circles indicate two synaptic contacts established by the neurone shown on the left side and one autaptic contact. They are shown at higher magnification in the right panels (*b*, *c* and *d* shown in *B*, *C* and *D*, respectively). The main axons of the two neurones are indicated by arrows; WM is white matter. *B*, presumed autaptic contact of a short axonal collateral (within the open circle) terminating on a secondary basal dendrite. *C*, *en passant* synaptic contact established on a tertiary basal dendrite. *D*, *en passant* synaptic contact on a secondary apical oblique dendrite. Axon collaterals are marked by arrows. All three contacts were identified as synapses by subsequent electron microscope analysis. Scale bars: 100 µm in *A*, 50 µm in *B-D*. Connection no. 21.

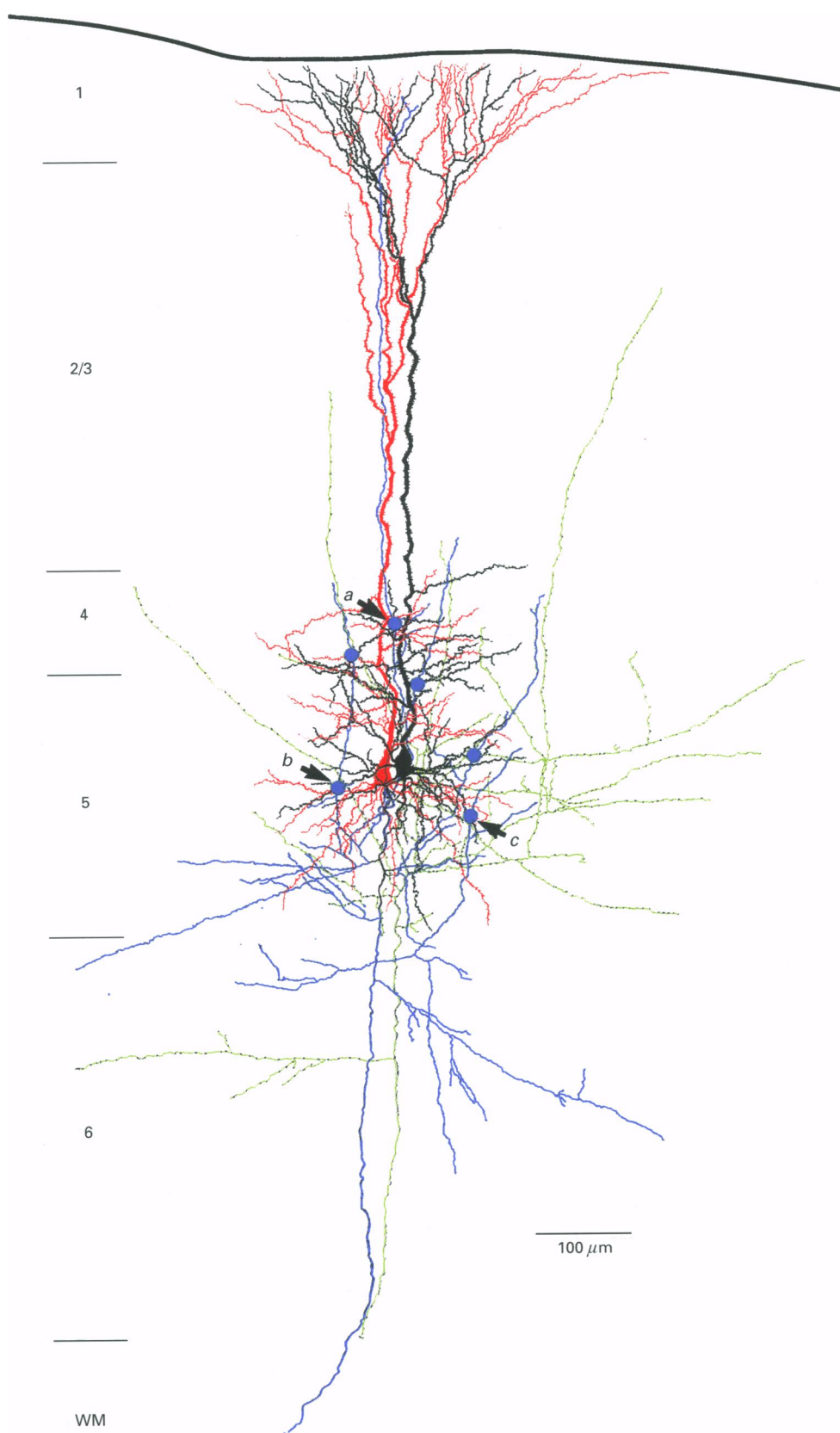


Figure 12. Camera lucida reconstruction of unidirectionally connected pair of neurones

Same neurones as shown in Fig. 11. The dendritic arbor of the projecting neurone is drawn in red, its axonal arbor in blue. The dendritic arbor of the target neurone is drawn in black, its axonal arborization in green. Blue circles indicate synaptic contacts established by the red/blue neurone at different dendritic locations on the black/green neurone. Arrows mark synaptic contacts which are shown in Fig. 14 at the electron microscopic level.

Table 1. Morphological quantification of unidirectionally connected neurones

		Projecting neurones	Target neurones
Somata	Vertical diameter (μm)	22.5 ± 2.9	22.3 ± 1.3
	Horizontal diameter (μm)	27.3 ± 2.1	29.9 ± 4.6
Dendrites	Number of basals	4.7 ± 0.5	5.1 ± 1.2
	Number of apical obliques	8.2 ± 1.1	8.3 ± 1.1
	Field span basals (μm)	308.7 ± 27.4	308.1 ± 17.8
	Field span apical obliques (μm)	279.5 ± 53.1	256.6 ± 25.2
	Field span terminal tuft (μm)	389.0 ± 44.7	359.8 ± 25.6
	Main apical length (μm)	479.6 ± 120.3	512.2 ± 128.9
	Distance from soma to apical oblique branch (μm)		
	1°	24.8 ± 11.0	36.2 ± 16.2
	2°	42.2 ± 18.1	57.8 ± 13.2
	3°	57.2 ± 18.1	72.5 ± 17.0
Axon collaterals	4°	57.9 ± 31.1	88.3 ± 16.6
	5°	114.3 ± 29.6	108.2 ± 20.4
	6°	126.4 ± 27.7	139.1 ± 32.2
	7°	154.9 ± 30.5	165.1 ± 33.5
	8°	188.4 ± 31.5	188.1 ± 28.3
	9°	229.9 ± 38.8	191.2 ± 34.2
	10°	280.0	174.0
	Number of horizontals	4.0 ± 1.1	4.1 ± 1.1
	Number of verticals	4.3 ± 1.1	4.0 ± 0.8
	Field span of horizontals (μm)	929.6 ± 117.3	984.3 ± 183.9
	Mean length of verticals (μm)	721.6 ± 252.7	679.3 ± 185.8

Morphology (means \pm s.d.) of neuronal dendrites, somata and axon collaterals in 14 neurones, connected unidirectionally. Field span refers to the maximal horizontal distance between dendrites or axon collaterals, respectively. The order of a dendrite is indicated by $^\circ$. 1° refers to the first branch originating from the soma or the main apical dendrite. For the oblique dendrites, starting from the 8° branch through to the 10° branch, the number of observations were 5, 3 and 1, respectively.

In addition, we examined to what extent synaptic contacts are located on the same dendrite. Out of forty identified synaptic contacts established by unidirectionally connected pyramidal neurones, ten (25%) were found on the same dendrite within a distance of $30 \mu\text{m}$ of each other.

Serial EM analysis was performed to confirm that potential contacts were indeed synaptic contacts. In a subpopulation of thirty-three contacts identified at the level of the light microscope, twenty-seven were verified at the EM level (the 6 remaining ones were not sectioned). Of the six potential synaptic contacts marked by blue circles in Fig. 12 all were verified as synaptic contacts at the EM level. Three axo-spinous synapses are shown, one on a secondary apical oblique dendrite (Fig. 14A) and two on secondary basal dendrites (Fig. 14B and C). A difficulty of the fine-structural analysis of synaptic contacts was that only neurones of which the soma was located within the upper $120 \mu\text{m}$ from the surface of the slice could be analysed. Neurones located more deeply in the slice could not be identified with certainty as thick tufted pyramidal neurones using IR-DIC visualization. This implied, however, that synaptic contacts of the biocytin-filled neurones were located in a zone of the

slice which may have been damaged during slice preparation (Frotscher, Misgeld & Nitsch, 1981). Hence, the fine-structural preservation of the tissue components, including the biocytin-labelled structures, was not perfect. Moreover, biocytin labelling of both the presynaptic and the postsynaptic element made the unequivocal identification of synaptic contacts difficult because the electron-dense reaction product obscured synaptic structures such as membrane specializations. The following criteria were applied for synapse identification at the EM level. (1) The presynaptic element contained accumulations of synaptic vesicles especially at presumed release sites. Synaptic vesicles are easily recognized because they do not contain reaction product and stand out as bright spots against the very electron-dense cytoplasm of the labelled axon terminal (Fig. 14A-C). (2) Pre- and postsynaptic membranes displayed the characteristic parallel apposition. (3) The synaptic cleft was wider than other membrane contacts and contained cleft material. (4) The postsynaptic element could be identified, e.g. as a spine, by its characteristic form (Fig. 14A-C). Postsynaptic elements were regarded as dendritic shafts if they were larger than spines and contained mitochondria.

Bidirectional synaptic connections. Six pairs of reconstructed pyramidal neurones that were bidirectionally coupled were also analysed in detail. Here, each neurone was a projecting and a target cell. Figure 15 illustrates a pair of bidirectionally coupled neurones at low magnification (Fig. 15*A*) and potential contact sites at different dendritic locations at higher magnification (Fig. 15*B–D*). The camera lucida reconstruction of this pair is shown in Fig. 16, illustrating that in this bidirectional connection each neurone established seven contacts, mostly on the basal and apical oblique dendrites of the other neurone. The morphological features of bidirectionally coupled neurones are detailed in Table 2. Statistical significance for different dendritic and axonal parameters of uni- and bidirectionally

connected neurones was tested for each pair (Wilcoxon signed-rank test) and this test confirmed that the sample of neurones investigated constituted a homogeneous class ($\alpha = 0.05$). The anatomical features of neurones that were bidirectionally coupled were also not different from those of unidirectionally coupled neurones (Tables 1 and 2).

The mean number of potential synaptic contacts formed on the target neurones (5.5 ± 1.1 ; range, 4–7 contacts) was not significantly different from unidirectionally coupled neurones, and the dendritic distribution of the synaptic contacts was also similar to that found on the target neurones of unidirectionally connected pairs. Of all the potential synaptic contacts identified, only a slightly higher percentage

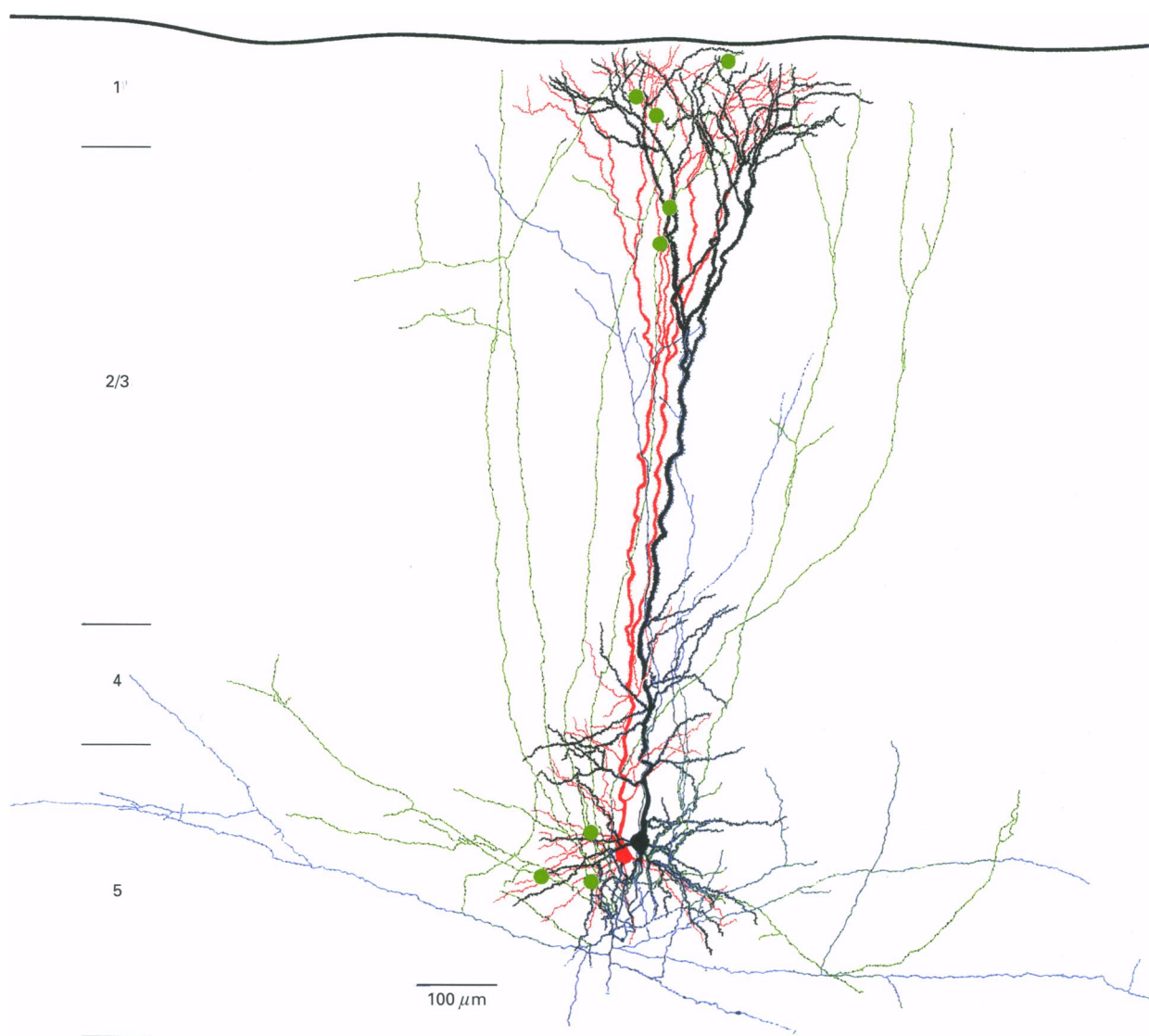


Figure 13. Synaptic contacts on apical tuft dendrites

Unidirectional synaptic connection. The dendritic arbor of the target neurone is drawn in red, its axonal arborization in blue. The dendritic morphology of the projecting neurone is drawn in black, the axonal arbor in green. The green circles indicate synaptic contacts established at different dendritic locations by the projecting (black/green) neurone on the target neurone (red/blue). Of the 8 contacts, 3 contacts are located on the terminal tuft and 2 contacts on the distal apical dendritic branches. Connection no. 10.

Table 2. Morphological quantification of bidirectionally connected neurones

		Rostral neurones	Caudal neurones
Somata	Vertical diameter (μm)	24.6 \pm 2.7	22.0 \pm 3.0
	Horizontal diameter (μm)	29.0 \pm 4.0	28.5 \pm 5.3
Dendrites	Number of basals	4.7 \pm 1.4	4.5 \pm 1.2
	Number of apical obliques	12.2 \pm 2.9	11.1 \pm 3.1
	Field span basals (μm)	288.7 \pm 17.2	311.8 \pm 25.6
	Field span apical obliques (μm)	273.2 \pm 27.2	275.7 \pm 30.6
	Field span terminal tuft (μm)	374.5 \pm 72.5	381.2 \pm 42.7
	Main apical length (μm)	478.9 \pm 169.3	448.9 \pm 148.2
	Distance from soma to apical oblique branch (μm)		
	1°	18.1 \pm 3.5	21.1 \pm 10.6
	2°	42.1 \pm 21.4	36.4 \pm 17.6
	3°	73.3 \pm 11.8	61.2 \pm 12.5
Axon collaterals	4°	49.9 \pm 9.1	77.0 \pm 16.3
	5°	124.3 \pm 12.8	103.7 \pm 25.5
	6°	149.8 \pm 14.0	127.6 \pm 12.4
	7°	133.7 \pm 9.0	161.6 \pm 30.4
	8°	181.7 \pm 11.5	176.9 \pm 34.3
	9°	200.5 \pm 13.1	189.8 \pm 37.3
	10°	209.4 \pm 9.5	234.4 \pm 42.1
	Number of horizontals	5.5 \pm 2.8	5.3 \pm 1.5
	Number of verticals	6.0 \pm 1.4	5.5 \pm 1.4
	Field span of horizontals (μm)	1023.4 \pm 250.0	1060.6 \pm 164.2
	Mean length of verticals (μm)	697.4 \pm 222.1	680.4 \pm 217.0
		Number (%)	Mean length (μm)
Axon collaterals forming synapses	1°	4 (8)	22
	2°	6 (12)	258
	3°	9 (18)	285
	4°	13 (26)	482
	5°	6 (12)	447
	6°	10 (20)	690
	7°	2 (4)	648

Morphology (means \pm s.d.) of neuronal dendrites, somata and axon collaterals of 12 neurones connected bidirectionally. Rostral neurone refers to neurones on the left side of figures (drawn in red in reconstructions), caudal neurones to those on the right side (drawn in black in reconstructions). Field span refers to the maximal horizontal distance between dendrites or axon collaterals. In the case of dendrites, ° refers to the order of a dendritic branch. 1° represents a branch originating from the soma or the main apical trunk. The 10° oblique dendritic branch is representative for 5 neurones. Six neurones had up to 12 apical obliques and 2 neurones had 17 apical obliques. Neurones were divided into rostral and caudal groups. The table also contains the morphological quantification of synapse-forming axon collaterals of 8 uni- or bidirectional connections. ° refers to the order of an axon collateral, 1° being the first collateral arising from the main axon. The mean distance of 1° branch points of the main axon from the soma was 129 μm . Number and % refer to the number of axon collaterals forming a synaptic contact and the percentage (50 observations).

(66.7%) of contacts was located on basal dendrites as compared with those observed in unidirectionally coupled pairs. This difference was primarily due to a tendency for synapse formation on quaternary dendritic branches (see also Table 3). Out of sixty-six potential synaptic contacts established between bidirectionally coupled layer 5 pyramidal neurones only fourteen (21.2%) were found on

the same dendrite. Serial EM analysis was employed to confirm synaptic contacts. Of the fourteen potential synaptic contact sites marked by blue and green circles in Fig. 16, eleven were found in EM sections and were verified as synaptic contacts at the EM level. One example of an axo-dendritic synaptic contact on each of the two neurones is shown in Fig. 17.

Innervation pattern. The uniformity of the anatomical characteristics of pyramidal cells was also evident in the pattern of innervation of the target by the projecting neurones derived from the pooled data of uni- and bidirectionally connected neurones. The mean length of an axon collateral of a projecting neurone forming a synaptic contact on basal dendrites of a target neurone was $250 \pm 69 \mu\text{m}$ ($n = 20$; range, 112 – $438 \mu\text{m}$) and the mean distance of the origin of 1st-order axon collaterals from the main axon origin was $129 \mu\text{m}$. The distribution of the order of the axon collaterals was non-random as most of the terminals were formed by 4th-order axon collaterals.

The pattern of synaptic innervation of a target neurone by a close-neighbour projecting neurone showed a preference for five to six synaptic contacts (Fig. 18*A*, inset) to be made on dendritic locations at a mean distance of $147 \mu\text{m}$ from the soma (median, $105 \mu\text{m}$, Fig. 18*A*). The mean distance on basal dendrites was $82 \pm 35 \mu\text{m}$ ($n = 67$), on apical oblique dendrites $145 \pm 59 \mu\text{m}$ ($n = 29$), and on the tuft $611 \pm 174 \mu\text{m}$ ($n = 10$; Table 3), and the distribution of the

location of synaptic contacts on dendritic branches showed a preference for 3rd-order branches (Table 3).

Number and dendritic location of contacts and synaptic efficacy. The mean unitary EPSP amplitudes varied over a 20-fold range in eighteen connections for which morphological reconstructions were made; the overall mean was 2.21 mV and the mean c.v. was 0.35 (in one of the anatomically characterized connections, the c.v. could not be determined), somewhat different from that of the larger sample of 138 connections (Fig. 4, open and filled bars; Fig. 7, large open circles and squares). The broad range of EPSP amplitudes could have indicated that individual connections varied widely in both number and dendritic location of their synaptic contacts. The unitary EPSP amplitude and the anatomically determined number of synaptic contacts (n_a) of a connection were, however, only weakly correlated (Fig. 18*B*) and EPSP amplitudes of a connection were also not correlated with the mean geometric distance (L) of the synaptic contacts from the soma (Fig. 18*C*).

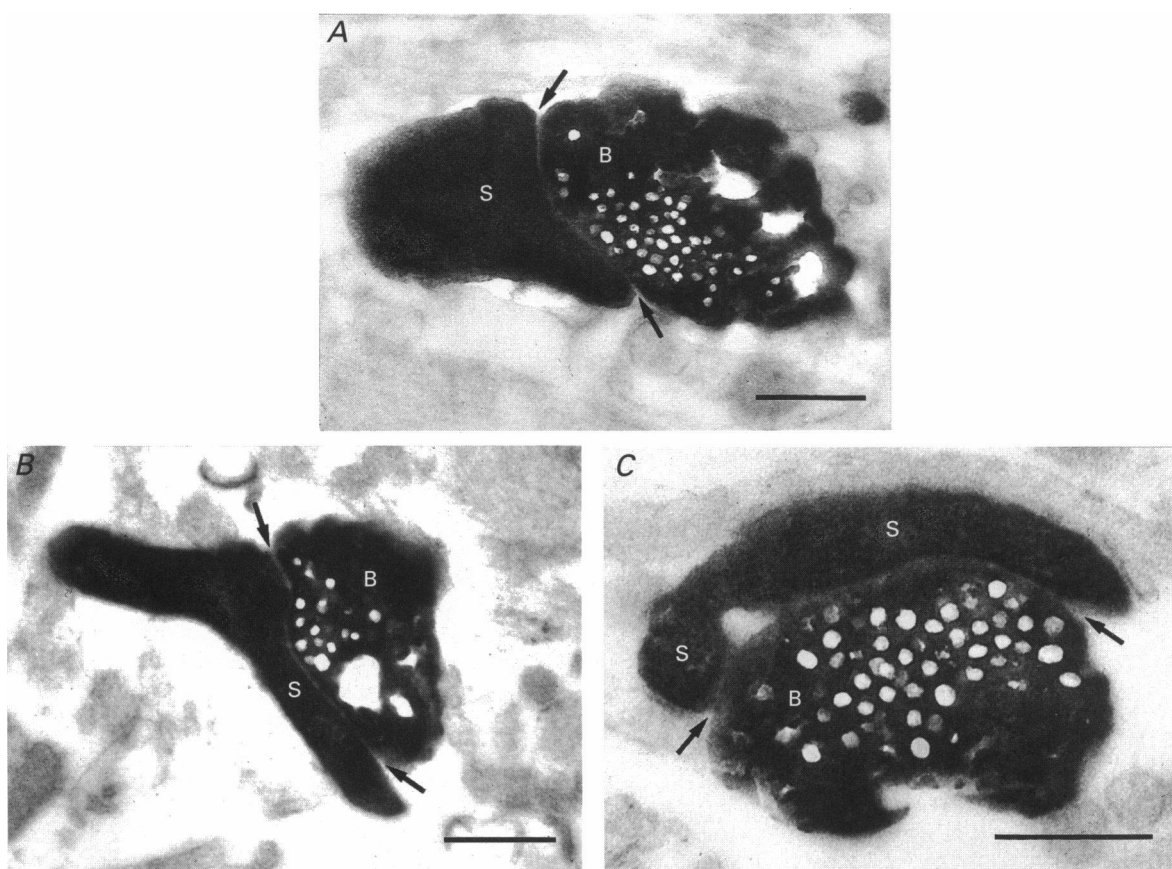


Figure 14. Electron microscopic identification of synaptic contacts

Three representative examples of the ultrastructure of potential synaptic contacts of the cell pair shown in Figs 11 and 12 (no. 21). *A*, axo-spinous contact established by one of the 'blue' axonal collaterals on a secondary apical oblique branch (*a* in Fig. 12). *B* and *C*, two axo-spinous contacts established on secondary basal dendrites (*b* and *c* in Fig. 12). Arrows point to the synaptic cleft. Note accumulation of synaptic vesicles, which do not contain reaction product, near the presumed active zone. B refers to synaptic bouton; S is spine. Scale bars in *A*–*C*, $0.5 \mu\text{m}$.

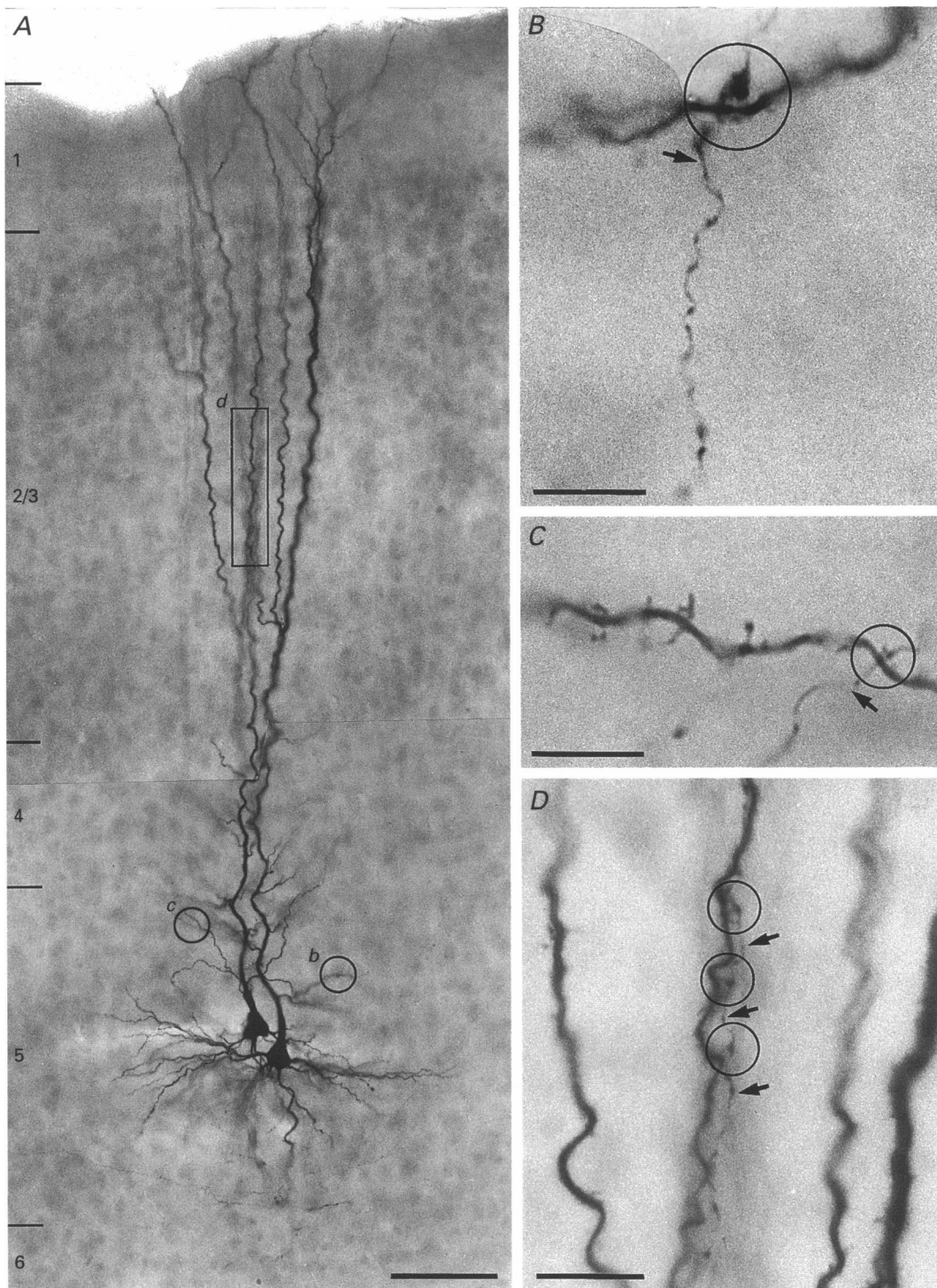


Figure 15. Bidirectionally connected pair of thick tufted pyramidal neurones

A, low magnification of a bidirectionally coupled pair of pyramidal neurones. The rectangular frame and circles indicate synaptic contacts of the two neurones (shown at higher magnification in the right panels). *B* and *C*, two examples of *en passant* synaptic contacts (with open circles) established on secondary apical oblique dendrites. *D*, two *en passant* synaptic contacts verified by electron microscopy on the main apical dendrite. Axonal collaterals are marked by arrows. The apposition in the middle was an autapse formed by this axon collateral. Scale bars: 100 µm in *A*, 50 µm in *B–D*. Connection no. 13.

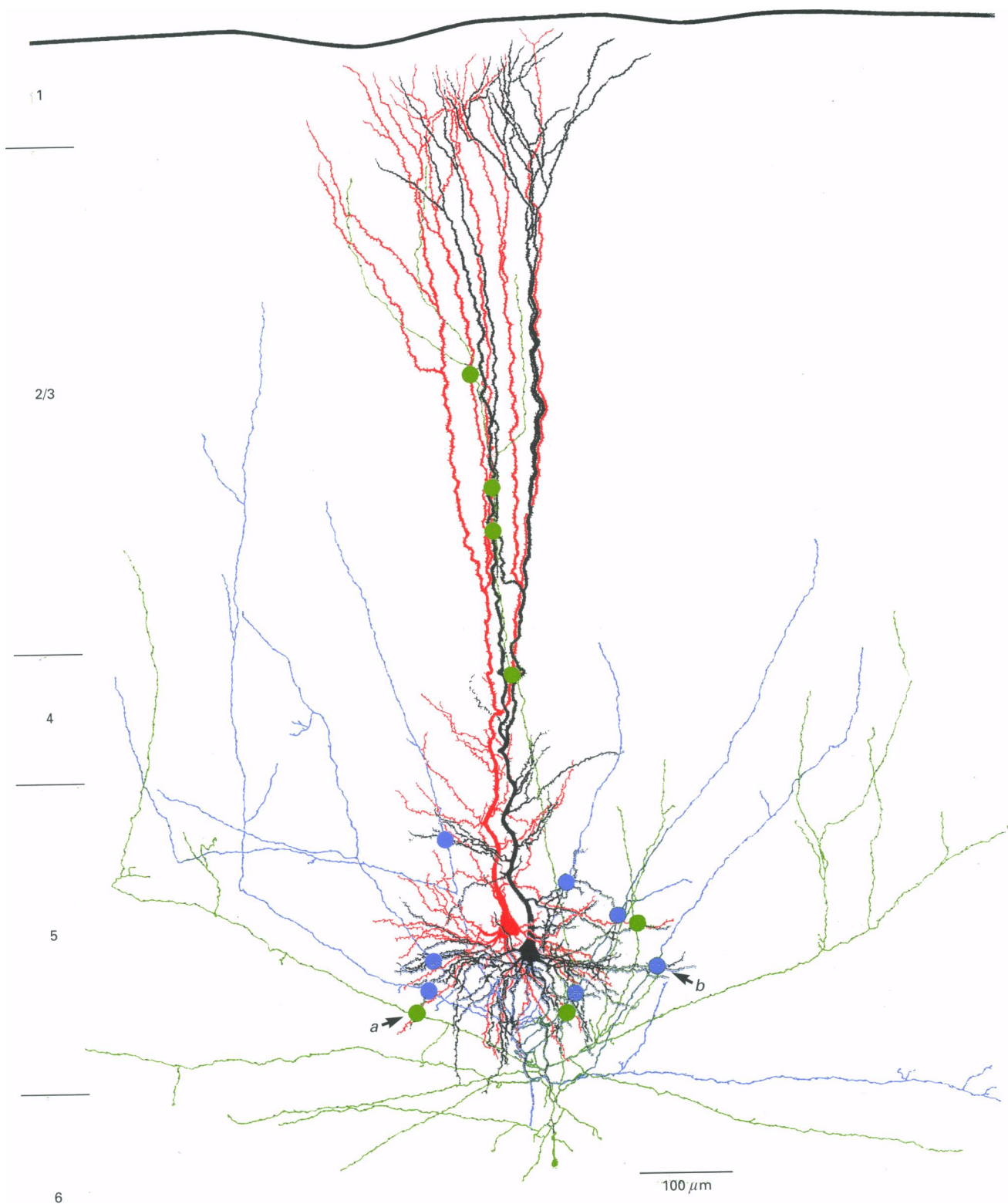


Figure 16. Camera lucida reconstruction of bidirectionally connected neurones

The two neurones shown in Fig. 15 were reconstructed. The dendritic arbor of one neurone is drawn in red and its axonal arborization in blue whereas the dendritic tree of the other neurone is black and its axonal arbor is green. Blue and green circles indicate synaptic contacts established by either the blue or the green axon at different dendritic locations. Each neurone established 7 synaptic contacts on the other neurone. Connection no. 13. Arrows mark synaptic contacts which are shown in Fig. 17 at the electron microscopic level.

Simulation of unitary EPSPs

To obtain a more precise view of how morphology on the one hand and pre- or postsynaptic functional mechanisms on the other determine the average unitary EPSP amplitude, its variability and the time course, we simulated EPSPs. Simulations were based on the assumption of a transmitter release mechanism which follows binomial statistics. Account was taken of the measured number and dendritic location of synaptic contacts and, in addition, specific compartmental models of neurones were used, which were based on camera lucida reconstructions of individual target neurones.

Release probability and size of quantal EPSPs. The c.v. of unitary EPSPs in eighteen anatomically reconstructed connections decreased strongly with the mean peak amplitude (Fig. 19A). As there is only a weak dependence of mean EPSP amplitude of the connection on the number of contacts or their mean geometric distance from the soma (Fig. 18B and C), this suggests that one major factor which could account for the large differences in the unitary EPSP amplitudes between different connections are differences in the transmitter release probability of the projecting neurones.

Estimates of the probability of evoked release, p_r , and the amplitude of quantal EPSPs measured at the soma, q_s , are obtained assuming that release follows binomial statistics (Katz, 1969) and assuming further that one presynaptic AP can evoke at each active

zone and the associated postsynaptic density only a single quantal EPSP either because only a single vesicle is released or because of postsynaptic receptor saturation (Korn, Sur, Charpier, Legendre & Faber, 1994; v. Kitzing, Jonas & Sakmann, 1994). The average size of the EPSP peak amplitude is given by $\Delta V = n_b p_r q_s$ where n_b represents the number of release sites. We assumed, for a first approximation, that n_b is given by the number of anatomically determined synaptic contacts n_a (Korn *et al.* 1994). To delineate the range of p_r and q_s for the eighteen connections, we used $n_a = 6$, the mean number of synaptic contacts (Fig. 19A), as the mean number of release sites. The release probability at synaptic contacts of a connection is estimated from the c.v. of its EPSP peak amplitudes, as $c.v. = \sqrt{[(1 - p_r)/(n_b p_r)]}$ and $p_r = 1/(1 + n_b(c.v.)^2)$. The estimate of q_s in each connection was derived as $q_s = \Delta V/n_b p_r$, assuming that for each synaptic contact of a connection the amplitude of quantal EPSPs at the soma was the same. This assumption seems justified for a first approximation because of the peaked distribution of distances of synaptic contacts from the soma (Fig. 18A).

Figure 19B (open symbols) shows that in connections with larger EPSP amplitudes (> 2 mV), the calculated release probability is higher than in connections with smaller EPSPs. Moreover, p_r seems to reach a limiting value, close to 0.9, corresponding to a mean quantal content of ~ 5 for these large EPSPs. Figure 19C (open symbols) shows that larger EPSP sizes could also imply larger values of q_s , increasing from 0.2 to 0.8 mV over the whole range.

The derived dependencies of p_r and q_s on EPSP amplitude (Fig. 19B and C, open symbols) are based on the assumption

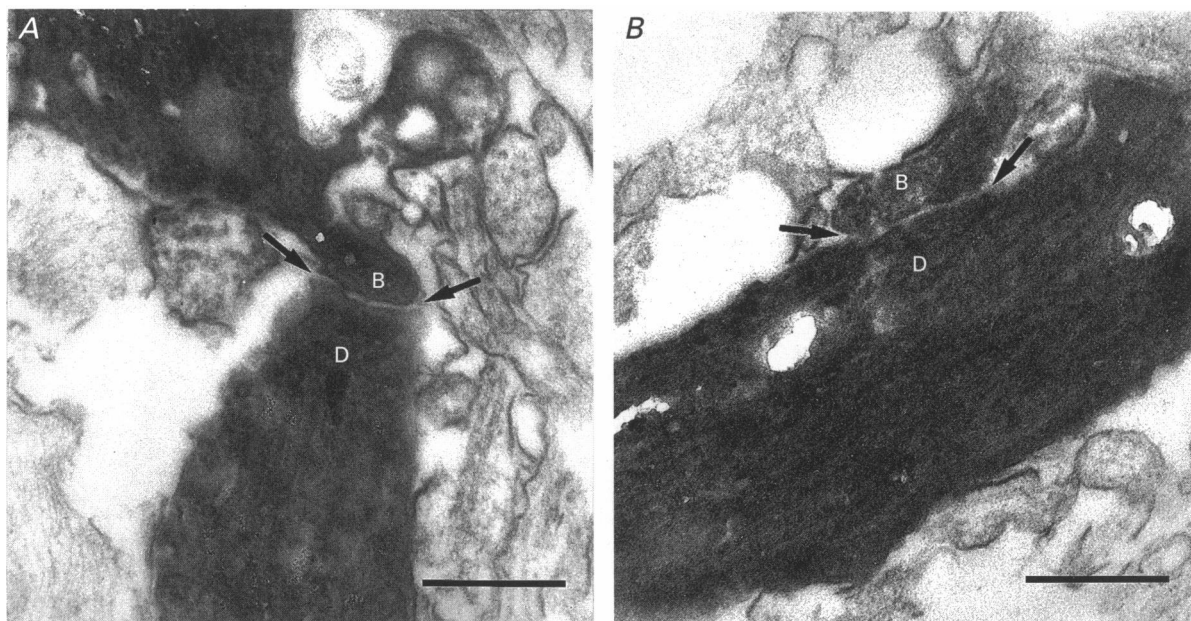


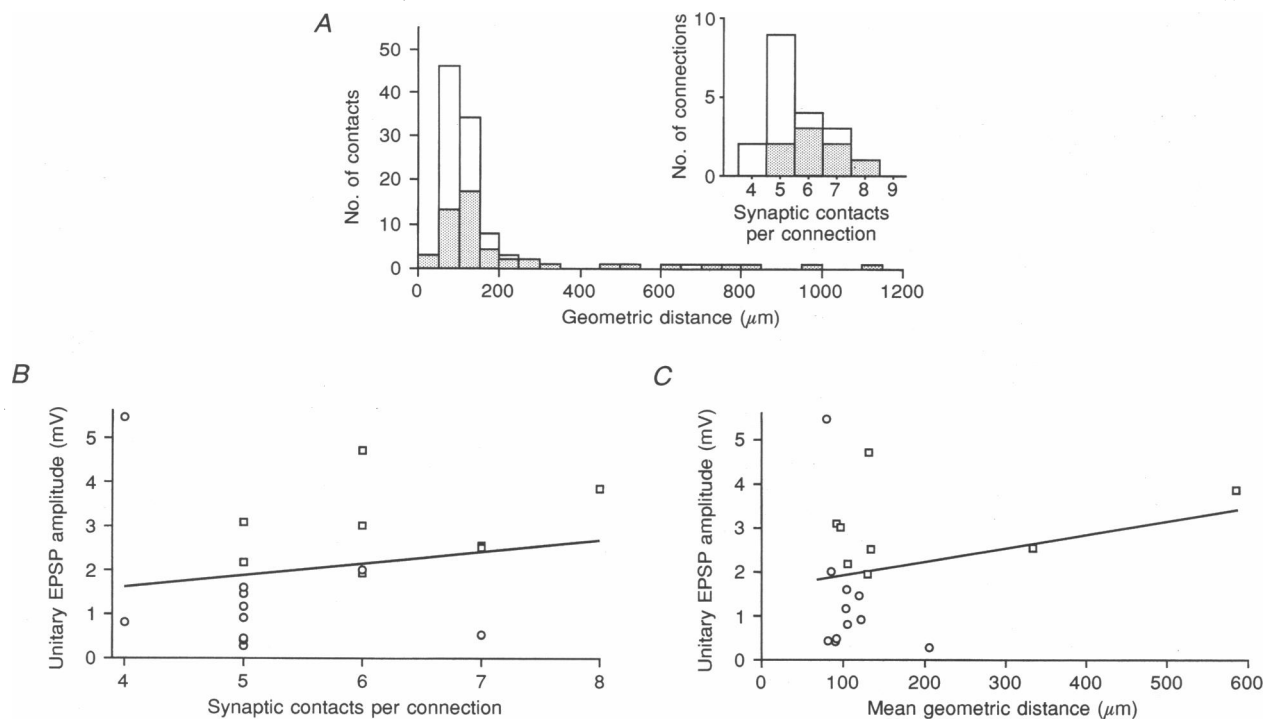
Figure 17. Electron microscopic identification of synaptic contacts between bidirectionally connected neurones

Examples of synaptic contacts established by each of the neurones (connection no. 13) illustrated in Figs 15 and 16. A, axo-dendritic contact established by a 'green' axonal collateral on a secondary basal ('red') dendrite, corresponding to the farthest left green circle marked *a* in Fig. 16. B, axo-dendritic contact established by a 'blue' axonal collateral on a secondary 'black' basal dendrite corresponding to farthest right blue circle marked *b* in Fig. 16. The arrows point to the synaptic cleft. B, synaptic bouton; D, dendrite. Scale bar, 1 μ m.

Table 3. Number and distance from soma of synaptic contacts in uni- and bidirectional synaptic connections

	Unidirectional connections			Bidirectional connections			Mean		
	Occurrence (% of total)	Distance from soma (μm)	n	Occurrence (% of total)	Distance from soma (μm)	n	Occurrence (% of total)	Distance from soma (μm)	n
Basal 1°	2.5	14.7	1	1.5	73.3	1	1.9	44.0 ± 35.2	2
Basal 2°	17.5	74.4 ± 17.9	7	15.2	75.6 ± 44.9	10	16.0	75.1 ± 35.3	17
Basal 3°	35.0	75.8 ± 20.5	14	34.8	86.9 ± 27.2	23	34.9	82.8 ± 25.2	37
Basal 4°	2.5	117.7	1	15.2	97.0 ± 30.7	10	10.4	98.3 ± 27.3	11
Oblique 1°	10.0	91.3 ± 14.9	4	4.4	184.6 ± 124.0	3	6.6	131.3 ± 87.4	7
Oblique 2°	15.0	134.0 ± 36.1	6	15.2	157.0 ± 59.1	10	15.1	151.1 ± 48.0	16
Oblique 3°	2.5	162.6	1	7.6	141.8 ± 54.7	5	5.7	145.3 ± 45.3	6
Main apical	7.5	598.2 ± 74.3	3	6.1	480.0 ± 140.9	4	6.6	530.8 ± 116.3	7
Terminal tuft	7.5	796.9 ± 104.7	3	0			2.8	796.9 ± 104.7	3

Nineteen synaptic connections between 26 neurones were examined: 7 between unidirectionally connected neurones and 12 between bidirectionally connected neurones. The number of putative synaptic contacts counted was 106. The percentage of the total number of synapses located on different dendritic sites and their mean distance from the soma are given. Total number of synaptic contacts was 40 in unidirectionally coupled neurones and 66 in bidirectionally coupled neurones. ° refers to the order of a dendritic branch. Basal 1° would be a dendrite arising from the soma, 1° oblique would be a dendrite arising from the main apical trunk.

**Figure 18.** Location of synaptic contacts on dendrites

A, histogram of geometric distances from the soma of synaptic contacts in 19 connections. Filled bars represent synaptic contacts in a subset of 8 connections which were used for simulations. Inset, distribution of number of synaptic contacts per connection (19 connections). B, plot of EPSP amplitude *versus* the number of synaptic contacts in a connection. The regression line has a slope of 0.27 mV per contact. The correlation coefficient is 0.2. Without the 'outlier' (4 contacts and 5.5 mV amplitude), the regression line has a slope of 0.63 mV per contact and a correlation coefficient of 0.51. C, plot of EPSP amplitude *versus* the geometric distance of synaptic contacts in a connection. The slope of the regression line is 3.2 mV mm⁻¹ and the correlation coefficient is 0.26. Same data set as in A and B.

of each contact representing one release site. To delineate the ranges of p_r and q_s more precisely, we selected those nine connections for analysis which had five identified synaptic contacts (Fig. 19D and E, open symbols). Fits of the c.v. versus EPSP amplitude relation with a single value of q_s were, however, also unsatisfactory, even with this further anatomical restriction. Upper and lower limits for q_s and p_r (Fig. 19D, continuous lines), suggested that p_r in this ensemble varied more than 5-fold, from 0.16 to 0.9 in the different connections (Fig. 19E, open symbols), whereas q_s varied only about 2-fold (Fig. 19F, open symbols). Neither

p_r nor q_s in this ensemble of connections were correlated significantly with the mean geometric distance of synaptic contacts from the soma (not shown). Thus, according to this analysis, with n_b assumed to be equal to anatomically determined n_a , the main factor responsible for the large variation in synaptic efficacy between morphologically homogeneous connections would be the difference in transmitter release probability of the projecting neurones, whereas differences in somatic quantal EPSPs contributed less significantly.

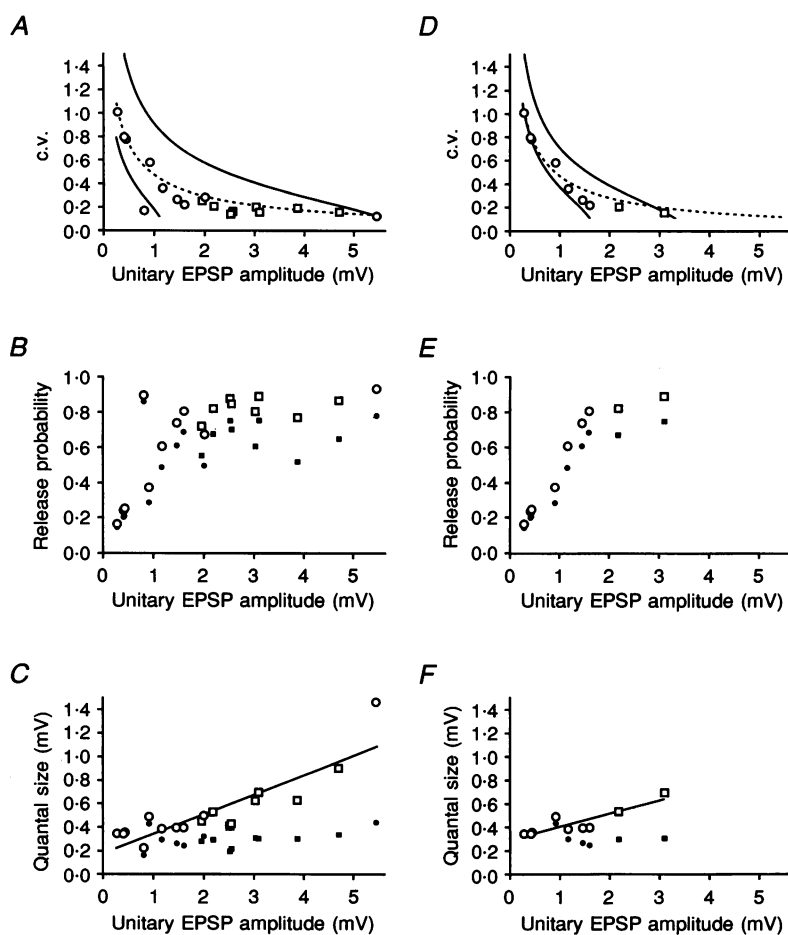


Figure 19. Determinants of synaptic efficacy

A, the coefficient of variation (c.v.) is plotted *versus* EPSP peak amplitude of 18 synaptic connections. Same data set as in Fig. 18 (except that in one connection, the c.v. could not be determined). The two continuous lines represent the prediction of binomial release statistics for $n_b = 6$, $q_s = 0.2$ mV (left) and $q_s = 1.0$ mV (right) as p_r increases from 0.15 (left) to 0.9 or from 0.06 to 0.9 (right). The p_r values refer to the two end-points of each curve. The dotted line represents the prediction when it was assumed that n_b/n_a increases linearly from 1 to 4 when EPSP amplitude increases from 0 to 5.5 mV. **B**, plot of derived p_r *versus* EPSP amplitude. Open symbols, $n_b/n_a = 1$. Filled symbols, n_b/n_a increases with EPSP size as in **A**. Same data set in **A-C**. **C**, plot of derived q_s *versus* EPSP amplitude, 18 connections. The regression line is fitted to open symbols, it has a slope of 0.17 and $n_b/n_a = 1$. Filled symbols, n_b/n_a increases with EPSP size as in **A**. **D**, plot of c.v. as a function of EPSP amplitude for 9 connections, each having 5 synaptic contacts. The two continuous lines represent the c.v. *vs.* EPSP relations expected for $n_b = 5$, $q_s = 0.34$ mV (left) and $q_s = 0.7$ mV (right) as p_r increases from 0.12 to 0.93 (left) or from 0.06 to 0.93 (right). The p_r values refer to the two end-points of each curve. Dotted line as in **A**. **E**, plot of p_r *versus* EPSP amplitude, 9 connections with 5 synaptic contacts each. Filled symbols as in **B**. **F**, plot of q_s *versus* EPSP amplitude, 9 connections with 5 synaptic contacts each. The regression line has a slope of 0.11. Filled symbols as in **C**. Same data set in **D-F**.

Synaptic efficacy is strongly dependent on the dendritic location of synaptic contacts as q_s represents an attenuated dendritic EPSP amplitude. Therefore, differences in the dendritic location of synaptic contacts could potentially contribute to the large variation in EPSP amplitudes. The q_s estimates were corrected for the differences in the individual geometric distances (L) of contacts from the soma. For the correction, an exponential attenuation (space constant = 370 μm , as determined from simulations of quantal EPSPs, see below) was used. The limiting ranges of q_s and p_r (Fig. 19D, continuous lines), which include all data points, were, however, only slightly (<10%) affected by this correction.

An alternative interpretation of the c.v. dependence on EPSP size could assume that the number of release sites, n_b , per anatomically determined synaptic contact increased linearly with the size of EPSPs (dotted lines in Fig. 19A and D and filled symbols in Fig. 19B, C, E and F). In this interpretation, the size of the quantal somatic EPSPs would vary only very little between different connections.

Dendritic EPSP attenuation. To delineate the dependence of synaptic efficacy on postsynaptic factors such as the dendritic location of synaptic contacts and the amplitude of the quantal conductance, detailed simulations of quantal and unitary EPSPs were made on eight connections using compartmental models of the target neurones with the more realistic assumption of a rapid dendritic quantal conductance transient. First, estimates of the electrotonic distances (X) of synaptic contacts from the soma were calculated from camera lucida reconstructions of the dendritic arbor. This is illustrated in Fig. 20, showing the geometric and electrotonic dendrogram of the target neurone of the cell pair shown in Figs 11 and 12. In this unidirectional connection, the six synaptic contacts on the target neurone were located at geometric distances between 79 and 235 μm from the soma, corresponding to electrotonic distances of 0.04–0.16.

Quantal EPSPs in the dendrite and soma were simulated using a 'standard' quantal conductance increase for each active contact. Depending on the location of the contact on the dendritic tree, quantal EPSPs at the soma of the target cell were strongly attenuated, by between 76 and 98% in different contacts. Somatic EPSP amplitudes were, however, almost uniform, differing in amplitudes by less than 1.5-fold (Fig. 21). Figure 22 summarizes the distribution of electrotonic distances (Fig. 22A), the dendritic attenuation of quantal EPSPs (Fig. 22B) and the quantal EPSP amplitudes at the soma (Fig. 22C) calculated for fifty synaptic contacts on eight target neurones. Dendritic EPSPs were attenuated at the soma, on average, by more than 20-fold and somatic quantal EPSP amplitudes varied over a 10-fold range for the same quantal conductance change, but only 2-fold for those generated at contacts located on basal and apical oblique dendrites. The distributions suggest that electrotonic distances of contacts from the soma on basal and apical oblique dendrites, and the attenuation and amplitudes of quantal EPSPs, are almost homogeneous in this ensemble (except for the connection with contacts on apical tuft dendrites: Fig. 13, connection no. 10rc). The variability of mean amplitudes was even less for simulated

unitary EPSPs (with comparable p_r values), which represent superpositions of about five quantal EPSPs because the differences of the constituting quantal EPSPs were averaged out. Thus, although the distances of synaptic contacts on dendrites from the soma of pyramidal neurones are potentially an important postsynaptic determinant of synaptic efficacy, they did not contribute significantly to the differences in efficacy between this set of eight pyramid–pyramid connections because of their uniform dendritic locations.

The connection illustrated in Fig. 13 (10rc) is an exception as synaptic contacts on the target neurone are located both on branches of the basal dendrites in layer 5 and on dendrites of the distal apical tuft in layer 1. Synaptic potentials in tuft synapses could be amplified by local dendritic calcium APs and the assumptions of passive attenuation of EPSPs may not hold for apical tuft dendrites (J. Schiller, Y. Schiller, G. Stuart & B. Sakmann, in preparation).

Quantal conductance increase. To obtain an estimate of the quantal conductance increase, unitary EPSPs were simulated for the eight connections with compartmental models of target neurones assuming binomial release statistics (Table 4). Depending on the coefficient of variation of the somatic amplitude of quantal EPSPs ((c.v.)_q), when using eqn (1) the values for p_r used for the simulations were increased between 0.02 (37rc) and 10% (10rc) with respect to the predictions of the simple binomial model with equivalent quantal contributions. The corrections using eqn (1) indicated that differences in the distribution of dendritic locations of synaptic contacts can contribute substantially to the measured c.v.s of somatic EPSP amplitudes (between 0.09 (37rc) and 23% (10rc), mean $4.8 \pm 7.7\%$), although they are unrelated to the release mechanism.

The peak of the transient conductance increase, g_q , was estimated by varying the size of g_q until experimental and simulated unitary EPSP amplitudes of a particular connection matched (Table 4). The quantal peak conductance ranged from 1.5 to 5.0 nS (excluding connection 10rc) with a mean of 3.0 nS.

Amplitude histograms. Simulations of unitary EPSPs indicate that quantal peaks corresponding to individual synaptic contacts would not be reliably detectable because of the variability in the somatic amplitude ((c.v.)_q) of the contributing quantal EPSPs, baseline noise and the high release probability in the connections simulated. Thus, even with the assumption of a small variability in peak conductance at a single contact and no variability between contacts, a more direct estimate of quantal conductance increase could not be obtained from the distributions of unitary EPSP amplitudes.

NMDAR channels. Simulations with a quantal conductance increase of 1.0 nS (AMPAR component) and an NMDAR component with 5.4 pS peak conductance at -60 mV, a 4.6 ms rise time constant and a 39 ms decay time constant suggested that the opening of NMDAR channels could contribute approximately 15% to the voltage integral of somatic unitary EPSPs at -60 mV, about 25% at -50 mV and about 50% at -30 mV. This is in the range observed experimentally (Fig. 9).

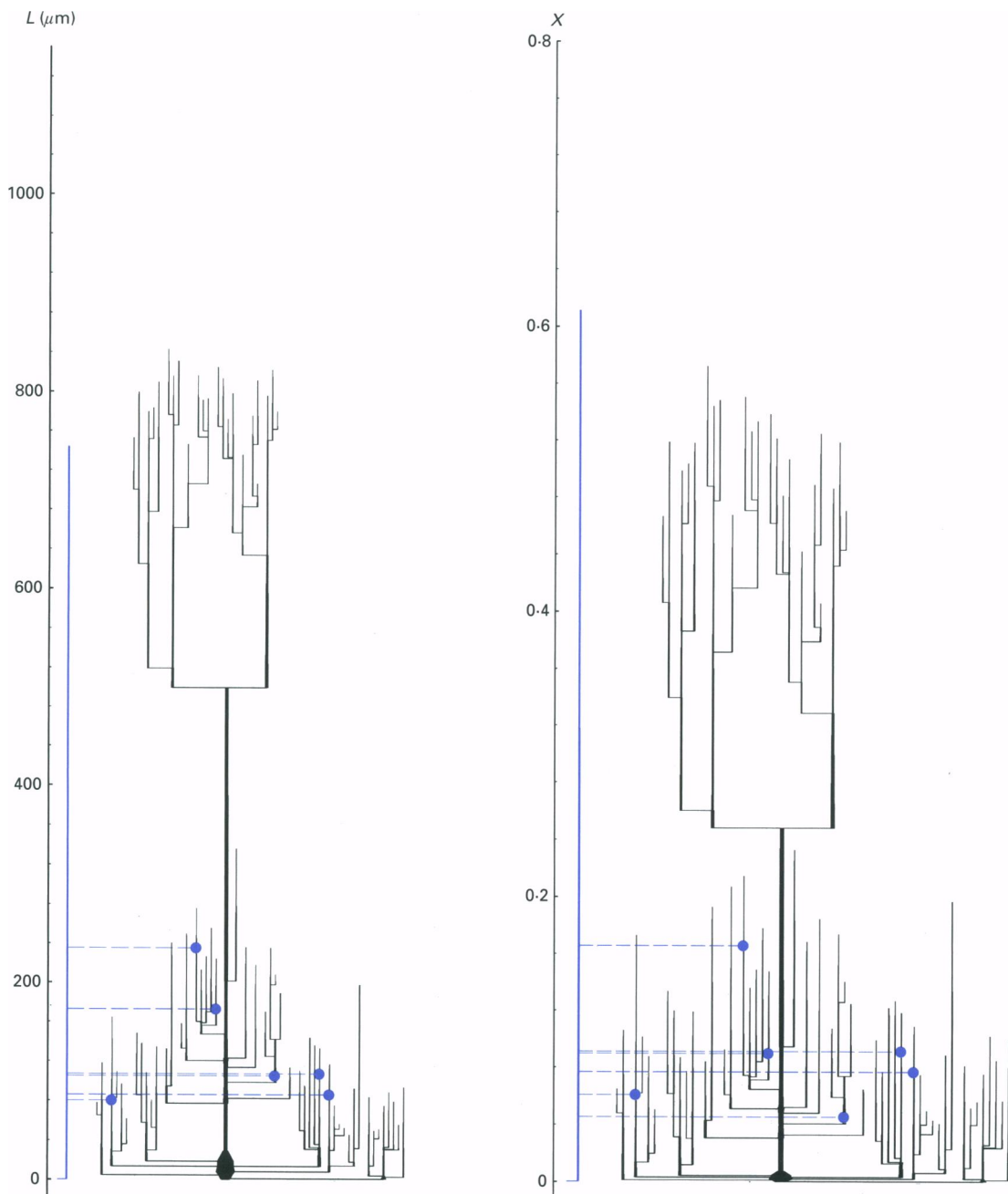


Figure 20. Geometric and electrotonic distances from the soma of synaptic contacts

Geometric and electrotonic dendograms of the target neurone drawn in black in Fig. 12. The electrotonic distance X of synaptic contacts (blue circles) from the soma is the sum of the electrotonic lengths $X_j = L_j/\lambda_j$ of the dendritic segments j leading to the location of the contact, where L_j is the geometric length of segment j and $\lambda_j = \sqrt{(R_m a_j/2R_i)}$ is the dendritic space constant. R_m and R_i were assumed to be $70\,000\, \Omega\, \text{cm}^2$ and $155\, \Omega\, \text{cm}$, respectively, and a_j is the mean radius of segment j . The geometric (L) and calculated electrotonic distances (X) of synaptic contacts were numbered, from left to right: No. 1, $79\, \mu\text{m}$, $0\cdot06$; No. 2, $235\, \mu\text{m}$, $0\cdot16$; No. 3, $172\, \mu\text{m}$, $0\cdot09$; No. 4, $104\, \mu\text{m}$, $0\cdot04$; No. 5, $106\, \mu\text{m}$, $0\cdot09$; No. 6, $85\, \mu\text{m}$, $0\cdot07$. The blue vertical line on the left represents, schematically, the main axon of the projecting neurone (drawn in red and blue in Fig. 12). Dashed lines represent, schematically, the axon collaterals of the projecting neurone. The axonal arbor of the target neurone is not shown.

Latency and time course of unitary EPSPs. The latency of a unitary EPSP, measured between the peak of the presynaptic AP at the soma and the onset of the somatic EPSP in the postsynaptic neurone depends on axonal conduction time, synaptic delay and dendritic delay. The length of axon collaterals between the main axon, presumably the initiation site for APs, and synaptic boutons was, on average, 400 μm . Assuming that the AP conduction velocity in axon collaterals is about 0.3 m s^{-1} , then the conduction time would be ~ 1.3 ms, about 2/3 of the latency of EPSPs when the conduction time from the AP initiation site in the main axon to the soma is neglected. Given that the electrotonic distance of most synaptic contacts from the soma is approximately 0.1, a dendritic delay of about 0.3 ms would be expected by electrotonic attenuation of EPSPs. As the mean latency was 1.9 ms in those connections for which the length of axon collaterals was determined, this leaves about 0.3 ms for the synaptic delay as measured between the peak of the presynaptic AP in the nerve terminal and the beginning of an EPSC.

Rise times of unitary EPSPs, simulated by activating quantal conductance changes at synaptic contacts located at

electrotonic distances ranging from 0.04 to 0.3, show that the expected 20–80% rise times of somatic EPSPs are around 1.6 ms (Fig. 21, Table 4). Temporal dispersion between quantal EPSPs at different synaptic contacts appears not to contribute significantly to rise times (but see 13 rc).

Decay times of unitary EPSPs are dependent on the duration of the quantal conductance change, and most significantly, on the electrotonic distance of synaptic contacts from the soma. Simulations with connections where contacts were located at mean electrotonic distances from the soma of 0.07–0.33 suggest that the decay time constant of unitary somatic EPSPs at -60 mV is significantly smaller than the passive membrane time constant. There is a fast component of the EPSP which is a residual of the strong (> 5 mV typically) and fast local EPSPs at the synaptic contacts during the synaptic conductance change (Fig. 21). The fast decay component of the somatic EPSP is more prominent if it is generated at synaptic contacts located at smaller electrotonic distances from the soma. A further acceleration of EPSP decay time course could be caused by the hyperpolarization-activated current (I_h).

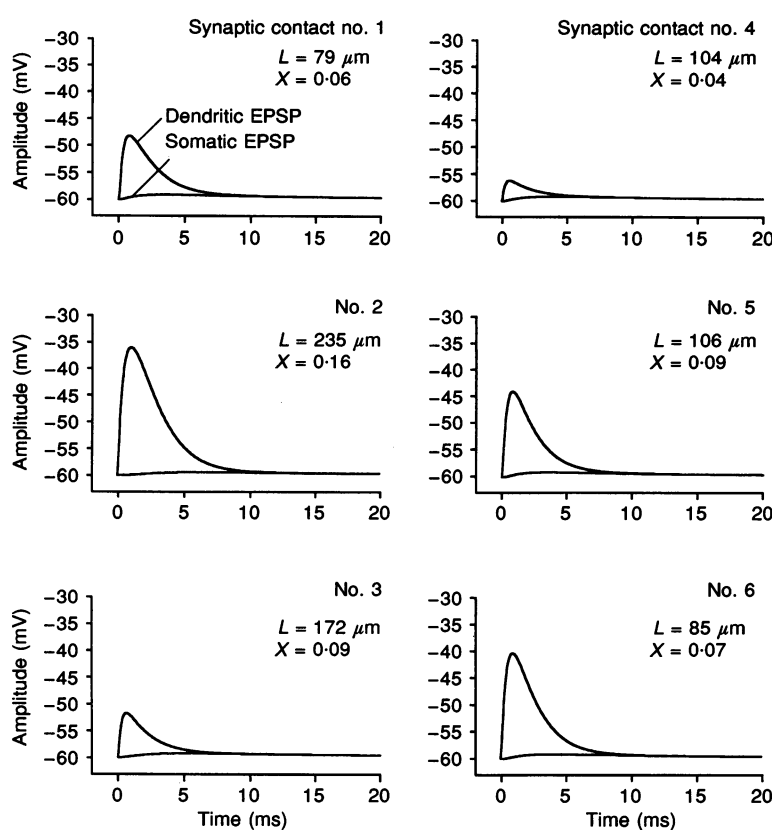


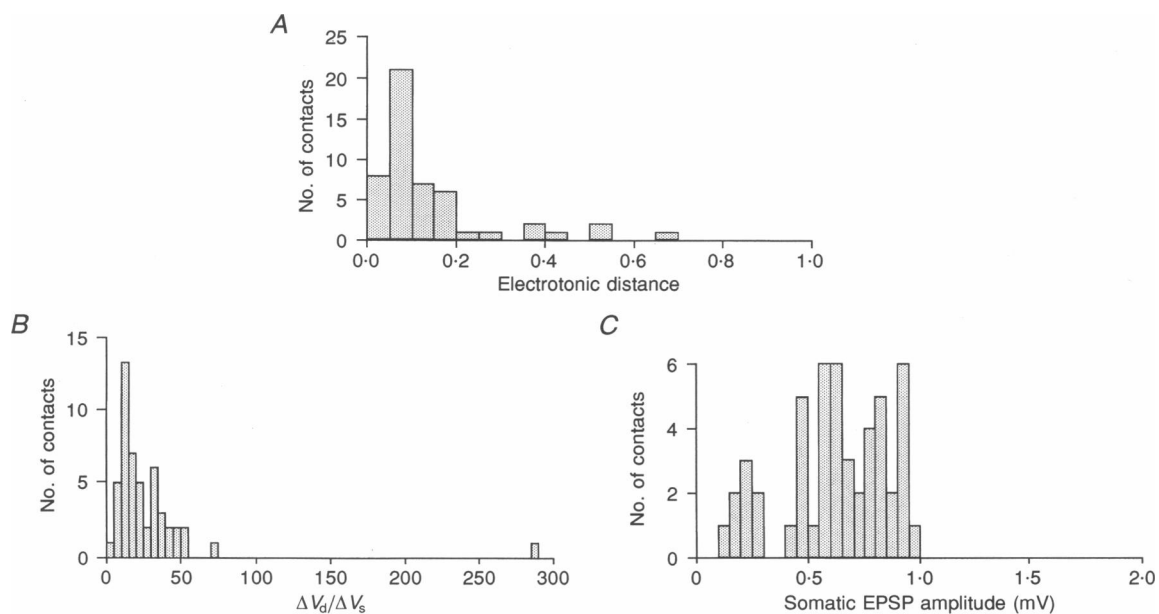
Figure 21. Simulation of quantal EPSPs in dendrite and soma

Simulated quantal EPSPs arising in 6 synaptic contacts located at different dendrites as shown in Fig. 20. For each contact the same quantal conductance change was assumed. Note large differences in dendritic EPSP peak amplitude at synaptic contacts in the spine head (between 3.8 and 23.9 mV) and of attenuation of EPSPs at the soma for the different contacts of this connection. Somatic quantal EPSPs varied between 0.57 and 0.94 mV.

Table 4. Summary of 8 completely reconstructed synaptic connections: unitary EPSPs

Identifier	Anatomy			Physiology					Simulation								
	Conn.	n_a	Mean L (μm)	Mean X	ΔV (mV)	c.v.	Lat.	rise time	τ	p_r	g_q (nS)	m	ΔV (mV)	$\Delta V_d/\Delta V_s$	Lat.	rise time	τ
37bc	6	95	0.067	3.0	0.20	1.2	3.2	44	0.81	2.20	4.9	3.0	17 ± 13	1.0	1.5	23 ± 4	
37rc	5	95	0.067	3.1	0.16	1.8	2.8	48	0.89	2.46	4.5	3.1	13 ± 2	1.3	1.2	23 ± 0.5	
36bc	6	131	0.09	4.7	0.16	1.0	2.4	25	0.87	5.03	5.2	4.7	22 ± 17	1.6	1.6	28 ± 8	
36rc	5	105	0.09	2.2	0.21	0.9	2.0	29	0.82	2.58	4.1	2.2	26 ± 15	1.6	1.7	20 ± 0.2	
21bc	6	130	0.09	2.0	0.25	2.0	3.6	51	0.73	1.45	4.4	1.9	18 ± 13	1.4	1.6	28 ± 4	
13bc	7	133	0.09	2.5	0.14	2.7	2.6	36	0.88	1.87	6.2	2.5	27 ± 13	1.2	1.7	24 ± 1.5	
13rc	7	334	0.19	2.6	0.16	1.8	4.4	38	0.87	3.17	6.1	2.5	29 ± 10	1.5	2.6	35 ± 13	
10rc	8	586	0.33	3.9	0.19	1.0	2.0	28	0.85	5.45	6.8	3.9	62 ± 94	1.1	1.6	37 ± 16	
Mean		6.25	201	0.13	3.0	0.18	1.55	2.87	37	0.84	3.03	5.3	3.0	27 ± 15	1.34	1.7	27 ± 6

Results of 8 completely reconstructed synaptic connections (Conn.; 2 unidirectional, 6 bidirectional). Anatomical (number of synaptic contacts, n_a) and physiological measurements (EPSP amplitude, ΔV and coefficient of variation (c.v.)) were used to estimate the size of the quantal conductance change, g_q , assuming that $n_b/n_a = 1$, taking into account the different electrotonic distances from the soma. τ is the EPSP decay time constant, $m = n_b p_r$ is the quantal content, and $\Delta V_d/\Delta V_s$ is the attenuation of quantal EPSPs (Fig. 22B). Lat., latency. Simulated $\Delta V_d/\Delta V_s$ and τ are given as means ± s.d. for quantal EPSPs originating from different synaptic contacts. For further details see text. Percentage of failures and c.v.s are shown in Fig. 7A and B (open squares). In each pair of connected cells, bc refers to black cell and rc refers to red cell in the camera lucida drawings.

**Figure 22. Electrotonic distances of synaptic contacts and attenuation of dendritic EPSPs**

A, histogram of calculated electrotonic distances from the soma of 50 synaptic contacts in 8 connections between neurones connected either unidirectionally ($n = 2$) or bidirectionally ($n = 6$). B, distribution of calculated attenuation of quantal EPSPs defined as the ratio of EPSP amplitude at the synaptic contact (ΔV_d) and at the soma (ΔV_s). C, distribution of simulated quantal EPSP amplitudes at the soma using a 'standard' conductance change of 2.7 nS peak amplitude arising from 50 synaptic contacts. The smallest group of quantal EPSPs arises exclusively from contacts located on dendrites of the apical tuft.

DISCUSSION

Dual recordings from pairs of thick tufted pyramidal neurones in layer 5 of juvenile rat neocortex revealed that each neurone is connected to at least 10% of the neighbouring pyramidal cells by fast excitatory synapses with glutamate as transmitter. Synaptic transmission was mediated by both AMPA and NMDA subclasses of glutamate receptors. The efficacy in these anatomically homogeneous connections varied by more than 20-fold and was reduced during bursts of presynaptic APs. The dominant factor responsible for the wide range of efficacies was the difference in transmitter release probability of the projecting neurones. In the following discussion, an attempt is made to dissect anatomical constraints and physiological mechanisms determining these properties.

Connectivity between layer 5 pyramidal cells. The probability of finding a synaptic connection in dual recordings in the brain slice preparation was considerably higher than previously reported for deep cortical layers. Nicoll & Blakemore (1990) found a 1:67 connection ratio in layer 5 and 1:70 was reported by Thomson, Deuchars & West (1993) between pyramidal neurones in layers 5 and 6. A 1:11 connection ratio has, however, been reported for layer 2/3 pyramidal cells (Mason *et al.* 1991) comparable to the ratio found here. The high ratio for layer 5 neurones could reflect a difference in the age of animals or, more likely, the fact that a more uniform population of neurones was examined when using IR-DIC optics to select neurones for paired recordings.

The pattern of evoking EPSPs by single APs may have excluded synaptic connections with more than 60% failures. However, nine pairs of unconnected neighbouring neurones were also filled with biocytin for morphological analysis and in five pairs either the axon or the apical dendrite was truncated, whereas in four pairs dendritic arborizations were extensive and no synaptic contacts were identified. This suggests that not all neighbouring pyramidal cells are connected but that the connection ratio of 1:10 is a lower estimate of the actual ratio of connections between neighbouring layer 5 pyramidal cells.

The physiological properties of unitary EPSPs, measured in 138 connections, as summarized in Figs 4 and 7, indicate that the mean values of peak amplitude, latency, rise and decay time constants are within the ranges reported for other intra- and interlaminar connections between other cortical neurones in rat motor or visual cortex (Mason *et al.* 1991; Thomson *et al.* 1993; Deuchars *et al.* 1994). From previous work, it is unclear whether the wide range of peak EPSP amplitudes reflected anatomical differences between individual connections within the same or different classes of neurones (Deuchars *et al.* 1994), or whether mostly functional differences of their synaptic contacts could account for these differences. To delineate the anatomical and/or functional factors that are responsible for the large differences in the efficacy of the pyramid–pyramid connections, we analysed their morphology in detail.

Morphologically uniform synaptic connections. The analysis of morphological features, as summarized in Tables 1–3, suggests that in this subset of layer 5 pyramidal cells connections were made between an anatomically homogeneous ensemble of thick tufted neurones.

A limitation of the brain slice preparation for determining the number of synaptic contacts is that recordings were made from neurones near the slice surface. This could lead to underestimation of the number of contacts and, in addition, very small synaptic contacts as well as contacts masked by the thick dendrites may have been omitted since only appositions clearly visible in the light microscope were counted. More than 80% of synapses selected in the light microscope were confirmed at the electron microscopic level, indicating that potential errors of identification of contacts may not be significant, but the average of five to six synaptic contacts per connection could be an underestimate of the real number.

These limitations are unlikely to affect significantly the measured dendritic distribution of synapses on different dendritic branches. Only 25% of synaptic contacts were located on the same dendritic branch; the remaining synaptic contacts were distributed over the dendritic tree, of which about 60% were located on basal dendrites and 50% of these on the 3rd-order branches of basal dendrites. This tendency to form synaptic contacts on 2nd- to 4th-order basal dendritic branches and a slight preference for these contacts to be established by 4th- to 5th-order axon collaterals may indicate a higher degree of specificity of the synaptic connection between neighbouring layer 5 pyramidal neurones than was previously assumed. Interestingly, the distribution pattern of autaptic contacts on dendrites of layer 5 neurones mirrors that of their synaptic contacts (Lübke, Markram, Frotscher & Sakmann, 1996).

Determinants of synaptic efficacy. For a synaptic connection between a single projecting neurone with one or several synaptic contacts on a single target neurone, the synaptic efficacy can be defined by the mean EPSP amplitude, $\Delta V = n_b p_r q_s$, when measured at a given membrane potential and not taking into account additional effects of non-linear summation of EPSPs and their voltage-dependent amplification (see below). In this simple form, synaptic efficacy is determined by presynaptic factors (n_b , p_r) referred to as ‘synaptic strength’ and a postsynaptic factor (q_s), assuming that all vesicles contain the same amount of transmitter (Korn, Faber & Triller, 1986). The relative contribution of release probability and quantal size to synaptic efficacy can be delineated assuming binomial release statistics, when the number of release sites is estimated assuming that n_b is equal to n_a , i.e. when there is only one release site per anatomically determined synaptic contact. Except for the seminal work of Korn & Faber and their associates on the goldfish brain (Korn *et al.* 1994, for review), this, to our knowledge, has not been done in a systematic way for other synaptic connections in the CNS.

We have set the number of release sites n_b equal to n_a , the number of synaptic contacts of projecting neurones, to derive both p_r and q_s from a c.v. analysis of unitary EPSP peak amplitudes in different connections. The fact that all synaptic contacts in pyramid–pyramid connections were located on dendrites complicated the derivation of p_r . Simulations demonstrated that differences in the dendritic locations of synaptic contacts could, in principle, substantially increase the variability (i.e. their c.v.) of measured unitary EPSP amplitudes. This source of variability is unrelated to the fluctuations in the release of vesicles from presynaptic boutons. Similarly, the dendritic location of synaptic contacts complicated the estimation of q_s as quantal EPSPs recorded at the soma may have to take into account up to 10-fold differences in amplitude of quantal EPSPs arising from the same conductance increase at contacts located on proximal or distal dendritic branches, although for most simulated connections, this range was only 2-fold.

According to the binomial analysis of unitary EPSPs in reconstructed connections, and assuming that n_b is equal to n_a (Fig. 19, Table 4), the main presynaptic determinant of the differences in the efficacy between different connections was the release probability, p_r , of the projecting neurones, whereas the differences in the number of synaptic contacts did not seem to contribute significantly, within the limited range of four to eight synaptic contacts. Differences on the postsynaptic side, such as the differences in quantal EPSP size (or rather the quantal conductance increase, g_q), were contributing less and the dendritic locations of contacts were almost homogeneous, located preferentially on basal or apical oblique dendrites, with the exception of one connection (no. 10, Fig. 13).

If the interpretation favoured here, that the release probability of the projecting neurones is the main factor responsible for the wide range of observed unitary EPSP amplitudes, also holds for the entire ensemble (Fig. 7), then there is no classification of the pyramid–pyramid connections possible into strong, intermediate or weak classes of connections as postulated for connections with layer 4 spiny stellate neurones of the cat cortex as target cells (Stratford, Tarczy-Hornoch, Martin, Bannister & Jack, 1996). Connections between layer 5 pyramids are characterized by a continuum of synaptic efficacies varying between weak (small EPSP and high c.v.) and strong (large EPSP and low c.v.). A different interpretation could be that those connections with the largest EPSP amplitudes constituted a separate class characterized by low c.v.s and, in addition, by larger g_q values.

The values of p_r and q_s were derived with the assumption that the number of release sites, n_b , is equal to n_a , the number of anatomically identified synaptic contacts. Alternatively, some boutons of synaptic contacts identified anatomically could have more than one release site, i.e. n_b is larger than n_a as measured by the number of boutons (Sorra & Harris, 1993; Korn *et al.* 1994). The c.v. *versus* unitary

EPSP plots (Figs 7 and 19) are also compatible with the assumption that the ratio of n_b/n_a increased from 1 to 4 with EPSP amplitude and that q_s is small and almost invariant. In this view, the connections with large EPSPs would form synaptic contacts with up to four release sites (each release site assumed to be represented by an active zone) per bouton. To clarify this issue, measurements by serial EM sectioning of synaptic contacts of the number of active zones in boutons of connections with low and high efficacy are necessary. Finally, the possibility must be considered that synaptic contacts or some active zones were functionally ‘silent’.

Several studies have reported differences in synaptic efficacy of individual connections of the same neuronal pathway (Mendell & Henneman, 1970; Mendell & Weiner, 1976; Miles, 1990; Raastad & Lipowski, 1996), but only few studies have attempted to correlate differences in synaptic efficacy with the number of release sites of the projecting neurone on the target cell. In the frog neuromuscular synapse, quantal content, as one measure of efficacy, was thought to be proportional to the length of the nerve terminal, implying a larger number of release sites for stronger connections (Kuno, Turkanis & Weakly, 1971). Detailed comparisons of the structure of nerve terminals and synaptic strength have, however, shown that motor units within the same or in different muscles have different ‘intrinsic’ release probabilities, depending on the particular motoneurone from which they arise (Grinnell & Trussell, 1983; Trussell & Grinnell, 1985). In inhibitory synaptic connections with the goldfish Mauthner cell, unitary IPSCs increase in amplitude with the number of contacts for weak connections with only a few (≤ 10) boutons, somewhat different from the observations on pyramid–pyramid connections described here. For the stronger connections, however, the quantal content of IPSCs is almost unrelated to the number of boutons, and synaptic efficacy is governed by differences in p_r (Korn *et al.* 1986).

Differences in synaptic efficacy of different projecting neurones on the same target neurone were found for Ia afferents to cat motoneurones (Mendell & Henneman, 1970; Mendell & Weiner, 1976) and for inhibitory connections made by interneurons projecting on pyramidal cells in the guinea-pig hippocampus (Miles, 1990) and were tentatively attributed to differences in n_a or p_r or both. For rat hippocampal CA3–CA1 pyramid synaptic connections via Schaffer collaterals (SC), the differences in synaptic efficacy between individual connections converging on the same CA1 pyramidal neurone were attributed to differences of both p_r and g_q (Raastad & Lipowski, 1996). In these connections synaptic efficacy is low in adult animals and it has been suggested that a developmental switch in efficacy from high to low occurs, which is based on a decrease in p_r (Bolshakov & Siegelbaum, 1995). Without anatomical reconstructions of projecting and target neurones, it seems, however, difficult to reach definite conclusions as to the contribution of the different factors determining efficacy and to decide which of

them are altered when efficacy either changes during development or is modified as a consequence of increased 'usage' of a connection (Stricker, Field & Redman, 1996*a,b*).

Quantal conductance increase. The simulations of unitary EPSPs, based on compartmental models of target neurones with identified synaptic contacts, indicated that the dendritic location of contacts is one important postsynaptic factor of efficacy, although for the connections of layer 5 pyramidal neurones, it did not contribute significantly to the differences between them. The estimated average quantal peak conductance (mean, 3 nS; Table 4) is comparable to that derived for rat hippocampal SC-CA1 pyramid connections (Stricker, Field & Redman, 1996*a*). It is substantially larger than that estimated for mossy fibre (MF)-CA3 pyramid synapses in the hippocampus (e.g. Jonas *et al.* 1993) or cerebellar MF-granule cell synapses (Silver, Cull-Candy & Takahashi, 1996), where synaptic contacts are located closer to the soma ($\leq 50\text{ }\mu\text{m}$) and the conductance increase was measured, more directly, under voltage clamp. The larger quantal conductance increase, in the range of several nanosiemens derived here, could be an overestimate because of several factors. Firstly, connections with particularly large unitary EPSPs were selected for simulations. Secondly, the number of physiologically active release sites, n_b , is larger than the number of anatomically determined synaptic contacts, n_a , either because of insufficient biocytin-filling of axon collaterals or because the boutons of the synaptic contact have more than one release site (Korn *et al.* 1994). In fact, if up to four release sites are assumed per bouton, the estimates of g_q would be in the range of those reported for MF-CA3 pyramid connections. Thirdly, the decay time course of the quantal conductance change which was used for EPSP simulations was too rapid as glutamatergic EPSCs may have an additional slow component (Silver *et al.* 1996) which could contribute significantly to the synaptic charge transfer. Finally, the validity of assumptions for simulations such as that of a largely passive electrical cable behaviour cannot be assessed at present. The derived values of the peak quantal conductance increase (Table 4) can therefore be regarded only as provisional estimates for a particular subset of horizontal synaptic connections with large EPSPs. Their validity must await direct quantal conductance measurements on dendrites and the determination of the number of active zones present in individual boutons.

Postsynaptic factors of efficacy. In addition to the location of synaptic contacts on the dendritic arbor, the passive membrane properties and the branching pattern of the dendrites, two other postsynaptic mechanisms could contribute to differences in efficacy. Both are dependent on the membrane potential of the target neurone. The effect of D-AP5, an antagonist of NMDAR channels, on amplitude and time course of EPSPs indicated that NMDARs contributed to unitary EPSPs. The dendritic depolarization caused by an AMPAR-mediated quantal conductance change could exceed 10 mV (Fig. 21) and this may be sufficient to

partially relieve NMDAR channels from Mg^{2+} block, at least at those synaptic contacts which are located close to the end of a dendrite (see for example Fig. 13). The contribution of the NMDAR-mediated current to the peak of unitary EPSPs at -60 mV is, however, expected to be small (<5%). A further postsynaptic factor that contributes to synaptic efficacy is voltage-dependent amplification of EPSPs which becomes operative close to AP threshold (Stuart & Sakmann, 1995).

Dynamic coupling of ensembles of pyramidal neurones. The field span of the horizontal axon collaterals of a pyramidal cell is close to 1 mm (Tables 1 and 2), defining a tissue cylinder in layer 5 which is about $50\text{ }\mu\text{m}$ in height containing one layer of the thick tufted neurones from which recordings were made. Given the dimensions of the neurones, a lower estimate of the average density of large thick tufted pyramidal neurones would be in the order of five per $10\,000\text{ }\mu\text{m}^2$ of cross-sectional area parallel to the cortical surface (assuming that neurones are about $45\text{ }\mu\text{m}$ apart). Consequently, at least around 400 potential target neurones would be available for each projecting pyramidal neurone. With the assumption of a uniform connection ratio of 1 : 10 this could indicate that a pyramidal neurone in layer 5 is coupled to at least 40 neighbouring pyramidal cells via synaptic connections as described here. Horizontal connections could contribute to synchronized electrical activity of ensembles of pyramidal neurones, for example during oscillations of electrical activity (Silva, Amitai & Connors, 1991). The synchronized excitatory input for ensemble activity may arise from the cortico-cortical association fibres forming excitatory synapses on the dendrites of the apical tuft. Via the horizontal axon collaterals, additional pyramidal neurones would then be recruited to ensemble electrical activity. As the field span of horizontal axon collaterals is about 1 mm, pyramidal neurones in different cortical columns could contribute to this recruitment. Depending on the efficacy of their connections, very different numbers of neighbouring neurones could cooperate to recruit additional synchronized APs in connected pyramidal neurones, ranging from more than 100 neurones for a synchronized ensemble of the weakly coupled neurones to as few as 5 for the strongly and reliably coupled neurones (such as those described in Table 4) if the threshold for AP initiation is 10–15 mV more positive than the measured resting potential.

The time delay between initiation of an AP in a presynaptic neurone and the peak of the EPSP close to the AP initiation site of the postsynaptic neurone (presumably the axon) is, at physiological temperature, in the range of 7–10 ms. This is an estimate of the jitter introduced by the horizontal connections for recruitment of additional neurones by the intralaminar excitatory circuits. Furthermore, the rapid depression of unitary EPSP amplitudes evoked by bursts of APs in the presynaptic neurone makes the efficacy of excitatory synaptic connections strongly dependent on the frequency pattern of AP activity. Depression could reflect

branch-point failures of APs in axon collaterals, as most synaptic boutons are formed by higher-order collaterals. Alternatively, a decrease of the release probability in terminals or slow recovery from desensitization of AMPA receptors in the postsynaptic membrane at those connections with high release probability could contribute to a reduction in efficacy. One functional consequence of depression could be that coincident burst-like electrical activity of ensembles of layer 5 pyramidal neurones would be most efficient in recruiting additional neurones to ensemble activity or in amplification of other excitatory inputs.

Perspectives

To elucidate those mechanisms which control the electrical behaviour of ensembles of synaptically connected pyramidal neurones in cortical layer 5, it will be necessary to investigate summation and amplification of unitary EPSPs in a single target neurone when APs in two or more neighbouring projecting neurones are elicited either synchronously or asynchronously. It will also be necessary to find out whether the wide range of unitary EPSP amplitudes in different connections reflects different distances between neurones or different stages of synapse development. Finally, it will be of interest to elucidate whether synchronous electrical activity of ensembles of pyramidal neurones can modify the synaptic efficacy of their horizontal connections and whether such changes in efficacy are a requirement for the formation or alteration of synaptic connections during development of the neocortex when functional cortical maps are established.

APPENDIX

Derivation of eqn (1)

Assuming that a connection has n_b release sites and each individual release site i can give rise to quantal EPSPs with amplitude q_i at the soma, and that the release probability p_r is the same for all release sites, the variance of the unitary EPSP amplitudes is given by:

$$\sigma^2 = \sum_{i=1}^{n_b} q_i^2 p_r(1 - p_r).$$

This can be rewritten as:

$$\sigma^2 = \sum_{i=1}^{n_b} (q_s + \Delta q_i)^2 p_r(1 - p_r),$$

where Δq_i are the deviations from the mean quantal size q_s ,

such that $\sum_{i=1}^{n_b} \Delta q_i = 0$. When expanded,

$$\sigma^2 = \sum_{i=1}^{n_b} (q_s^2 + \Delta q_i^2) p_r(1 - p_r),$$

it can be reformulated in terms of the coefficient of variation of the quantal sizes, $(c.v.)_q$:

$$\sigma^2 = n_b q_s^2 (1 + (c.v.)_q^2) p_r(1 - p_r).$$

Consequently, the c.v. of the unitary EPSP amplitudes is:

$$(c.v.)^2 = \frac{\sigma^2}{n_b^2 p_r^2 q_s^2} = \frac{(1 + (c.v.)_q^2)(1 - p_r)}{n_b p_r},$$

which can be inverted to yield the release probability at each contact:

$$p_r = \frac{1 + (c.v.)_q^2}{1 + (c.v.)_q^2 + n_b (c.v.)^2}.$$

- BARTOL, T. M., LAND, B. R., SALPETER, E. E. & SALPETER, M. M. (1991). Monte Carlo simulation of miniature endplate current generation in the vertebrate neuromuscular junction. *Biophysical Journal* **59**, 1290–1307.
- BOLSHAKOV, V. Y. & SIEGELBAUM, S. A. (1995). Regulation of hippocampal transmitter release during development and long-term potentiation. *Science* **269**, 1730–1734.
- BORST, J. G. G. & SAKMANN, B. (1996). Calcium influx and transmitter release in a fast CNS synapse. *Nature* **383**, 431–434.
- BURNASHEV, N., ZHOU, Z., NEHER, E. & SAKMANN, B. (1995). Fractional calcium currents through recombinant GluR channels of the NMDA, AMPA and kainate receptor subtypes. *Journal of Physiology* **485**, 403–418.
- CHAGNAC-AMITAI, Y., LUHMANN, H. J. & PRINCE, D. A. (1990). Burst generating and regular spiking layer 5 pyramidal neurons of rat neocortex have different morphological features. *Journal of Comparative Neurology* **296**, 598–613.
- CONNORS, B. W. & GUTNICK, M. J. (1990). Intrinsic firing pattern of diverse neocortical neurons. *Trends in Neurosciences* **13**, 99–104.
- DEFELIPE, J. & FARINAS, I. (1992). The pyramidal neuron of the cerebral cortex: morphological and chemical characteristics of the synaptic inputs. *Progress in Neurobiology* **39**, 563–607.
- DEISZ, R. A., FORTIN, G. & ZIEGLGÄNSBERGER, W. (1991). Voltage dependence of excitatory postsynaptic potentials of rat neocortical neurons. *Journal of Neurophysiology* **65**, 371–382.
- DEUCHARS, J., WEST, D. C. & THOMSON, A. M. (1994). Relationships between morphology and physiology of pyramid–pyramid single-axon connections in rat neocortex *in vitro*. *Journal of Physiology* **478**, 423–435.
- FABER, D. S. & KORN, H. (1991). Applicability of the coefficient of variation method for analyzing synaptic plasticity. *Biophysical Journal* **60**, 1288–1294.
- FROTSCHER, M., MISGELD, U. & NITSCH, C. (1981). Ultrastructure of mossy fiber endings in *in vitro* hippocampal slices. *Experimental Brain Research* **41**, 247–255.
- GILBERT, C. D. & WIESEL, T. N. (1979). Morphology and intracortical projections of functionally characterised neurones in the cat visual cortex. *Nature* **280**, 120–125.
- GRINNELL, A. D. & TRUSSELL, L. O. (1983). Synaptic strength as a function of motor unit size in the normal frog sartorius. *Journal of Physiology* **338**, 221–241.
- HINES, M. (1993). NEURON – a program for simulation of nerve equations. In *Neural Systems: Analysis and Modeling*, ed. ECKMAN, F., pp. 127–136. Kluwer Academic Publishers, Norwell, MA, USA.
- JONAS, P., MAJOR, G. & SAKMANN, B. (1993). Quantal components of unitary EPSCs at the mossy fibre synapse on CA3 pyramidal cells of rat hippocampus. *Journal of Physiology* **472**, 615–663.

- JONAS, P., RACCA, C., SAKMANN, B., SEEBURG, P. H. & MONYER, H. (1994). Differences in Ca^{2+} permeability of AMPA-type glutamate receptor channels in neocortical neurons caused by differential GluR-B subunit expression. *Neuron* **12**, 1281–1289.
- KASPER, E. M., LARKMAN, A. U., LÜBKE, J. & BLAKEMORE, C. (1994a). Pyramidal neurons in layer 5 of the rat visual cortex. I. Correlation among cell morphology, intrinsic electrophysiological properties, and axon targets. *Journal of Comparative Neurology* **339**, 459–474.
- KASPER, E. M., LÜBKE, J., LARKMAN, A. U. & BLAKEMORE, C. (1994b). Pyramidal neurons in layer 5 of the rat visual cortex. III. Differential maturation of axonal targeting, dendritic morphology, and electrophysiological properties. *Journal of Comparative Neurology* **339**, 495–518.
- KATZ, B. (1969). *The Release of Neural Transmitter Substances*. Liverpool University Press, Liverpool.
- KORN, H., FABER, D. S. & TRILLER, A. (1986). Probabilistic determination of synaptic strength. *Journal of Neurophysiology* **55**, 402–421.
- KORN, H., SUR, C., CHARPIER, S., LEGENDRE, P. & FABER, D. S. (1994). The one-vesicle hypothesis and multivesicular release. In *Molecular and Cellular Mechanisms of Neurotransmitter Release*, ed. STJÄRNE, L., GREENGARD, P., GRILLNER, S., HÖKFELT, T. & OTTOSON, D., pp. 301–322. Raven Press, New York.
- KUNO, M., TURKANIS, S. A. & WEAKLY, J. N. (1971). Correlation between nerve terminal size and transmitter release at the neuromuscular junction of the frog. *Journal of Physiology* **213**, 545–556.
- LARKMAN, A. & MASON, A. (1990). Correlations between morphology and electrophysiology of pyramidal neurons in slices of rat visual cortex. I. Establishment of cell classes. *Journal of Neuroscience* **10**, 1407–1414.
- LÜBKE, J., MARKRAM, H., FROTSCHER, M. & SAKMANN, B. (1996). Frequency and dendritic distribution of autapses established by layer 5 pyramidal neurons in the developing rat neocortex: comparison with synaptic innervation of adjacent neurons of the same class. *Journal of Neuroscience* **16**, 3209–3218.
- MARKRAM, H. & SAKMANN, B. (1994). Calcium transients in dendrites of neocortical neurons evoked by single subthreshold excitatory postsynaptic potentials via low-voltage-activated calcium channels. *Proceedings of the National Academy of Sciences of the USA* **91**, 5207–5211.
- MASON, A. & LARKMAN, A. (1990). Correlations between morphology and electrophysiology of pyramidal neurons in slices of rat visual cortex. II. Electrophysiology. *Journal of Neuroscience* **10**, 1415–1428.
- MASON, A., NICOLL, A. & STRATFORD, K. (1991). Synaptic transmission between individual pyramidal neurons of the rat visual cortex *in vitro*. *Journal of Neuroscience* **11**, 72–84.
- MENDELL, L. M. & HENNEMAN, E. (1970). Terminals of single Ia fibers: Location, density, and distribution within a pool of 300 homonymous motoneurons. *Journal of Neurophysiology* **34**, 171–187.
- MENDELL, L. M. & WEINER, R. (1976). Analysis of pairs of individual Ia-e.p.s.p.s in single motoneurones. *Journal of Physiology* **255**, 81–104.
- MILES, R. (1990). Variation in strength of inhibitory synapses in the CA3 region of guinea-pig hippocampus *in vitro*. *Journal of Physiology* **431**, 659–676.
- MONYER, H., SPRENGEL, R., SCHOEPFER, R., HERB, A., HIGUCHI, M., LOMELI, H., BURNASHEV, N., SAKMANN, B. & SEEBURG, P. H. (1992). Heteromeric NMDA receptors: Molecular and functional distinction of subtypes. *Science* **256**, 1217–1221.
- NICOLL, A. & BLAKEMORE, C. (1990). Dual intracellular impalement *in vitro* reveals excitatory synaptic connections between pyramidal neurones in rat visual cortex. *Journal of Physiology* **430**, 15P.
- NICOLL, A., LARKMAN, A. & BLAKEMORE, C. (1993). Modulation of EPSP shape and efficacy by intrinsic membrane conductances in rat neocortical pyramidal neurons *in vitro*. *Journal of Physiology* **468**, 693–710.
- PETERS, A. & KAISERMAN-ABRAMOF, I. R. (1970). The small pyramidal neuron of the rat cerebral cortex: The perikaryon, dendrites and spines. *American Journal of Anatomy* **127**, 321–356.
- RAASTAD, M. & LIPOWSKI, R. (1996). Diversity of postsynaptic amplitude and failure probability of unitary excitatory synapses between CA3 and CA1 cells in the rat hippocampus. *European Journal of Neuroscience* **8**, 1265–1274.
- RAMÓN Y CAJAL, S. (1911). *Histologie du Système Nerveux de l'Homme et des Vertebrés*. Maloine, Paris.
- SILVA, L. R., AMITAI, Y. & CONNORS, B. W. (1991). Intrinsic oscillations of neocortex generated by layer 5 pyramidal neurons. *Science* **251**, 432–435.
- SILVER, R. A., CULL-CANDY, S. G. & TAKAHASHI, T. (1996). Non-NMDA glutamate receptor occupancy and open probability at a rat cerebellar synapse with single and multiple release sites. *Journal of Physiology* **494**, 231–250.
- SORRA, K. E. & HARRIS, K. M. (1993). Occurrence and three-dimensional structure of multiple synapses between individual radiatum axons and their target pyramidal cells in hippocampal area CA1. *Journal of Neuroscience* **13**, 3736–3748.
- SPAIN, W. J., SCHWINDT, P. C. & CRILL, W. E. (1987). Anomalous rectification in neurons from cat sensorimotor cortex *in vitro*. *Journal of Neurophysiology* **57**, 1555–1576.
- SPRUSTON, N. & JOHNSTON, D. (1992). Perforated patch-clamp analysis of the passive membrane properties of three classes of hippocampal neurons. *Journal of Neurophysiology* **67**, 508–529.
- STAFFSTROM, C. E., SCHWINDT, P. C. & CRILL, W. E. (1982). Negative slope conductance due to a persistent subthreshold sodium current in cat neocortical neurons *in vitro*. *Brain Research* **236**, 221–226.
- STRATFORD, K. J., TARCY-HORNOCH, K., MARTIN, K. A. C., BANNISTER, N. J. & JACK, J. J. B. (1996). Excitatory synaptic inputs to spiny stellate cells in cat visual cortex. *Nature* **382**, 258–261.
- STRICKER, C., FIELD, A. C. & REDMAN, S. J. (1996a). Statistical analysis of amplitude fluctuations in EPSCs evoked in rat CA1 pyramidal neurones *in vitro*. *Journal of Physiology* **490**, 419–441.
- STRICKER, C., FIELD, A. C. & REDMAN, S. J. (1996b). Changes in quantal parameters of EPSCs in rat CA1 neurones *in vitro* after the induction of long-term potentiation. *Journal of Physiology* **490**, 443–454.
- STUART, G. J., DODT, H.-U. & SAKMANN, B. (1993). Patch-clamp recordings from the soma and dendrites of neurons in brain slices using infrared video microscopy. *Pflügers Archiv* **423**, 511–518.
- STUART, G. & SAKMANN, B. (1995). Amplification of EPSPs by axosomatic sodium channels in neocortical pyramidal neurons. *Neuron* **15**, 1065–1076.
- THOMSON, A. M. & DEUCHARS, J. (1994). Temporal and spatial properties of local circuits in neocortex. *Trends in Neurosciences* **17**, 119–126.
- THOMSON, A. M., DEUCHARS, J. & WEST, D. C. (1993). Large, deep layer pyramid–pyramid single-axon EPSPs in slices of rat motor cortex display paired pulse and frequency-dependent depression, mediated presynaptically and self-facilitation, mediated post-synaptically. *Journal of Neurophysiology* **70**, 2354–2369.

- THOMSON, A. M. & WEST, D. C. (1993). Fluctuations in pyramid-pyramid excitatory postsynaptic potentials modified by presynaptic firing pattern and postsynaptic membrane potential using paired intracellular recordings in rat neocortex. *Neuroscience* **54**, 329–346.
- TRUSSELL, L. O. & GRINNELL, A. D. (1985). The regulation of synaptic strength within motor units of the frog cutaneous pectoris muscle. *Journal of Neuroscience* **1**, 243–254.
- VALVERDE, F. (1986). Intrinsic neocortical organization: Some comparative aspects. *Neuroscience* **18**, 1–23.
- v. KITZING, E., JONAS, P. & SAKMANN, B. (1994). Quantal analysis of excitatory postsynaptic currents at the hippocampal mossy fiber-CA3 pyramidal cell synapse. In *Molecular and Cellular Mechanisms of Neurotransmitter Release*, ed. STJÄRNE, L., GREENGARD, P., GRILLNER, S., HÖKFELT, T. & OTTOSON, D., pp. 235–260. Raven Press, New York.
- WANG, Z. & McCORMICK, D. A. (1993). Control of firing mode of corticotectal and corticopontine layer V burst-generating neurons by norepinephrine, acetylcholine, and *1S,3R*-ACPD. *Journal of Neuroscience* **13**, 2199–2216.

Acknowledgements

We thank Professors D. Colquhoun and P. Jonas and Drs J. G. G. Borst, E. v. Kitzing and A. D. Reyes for their critical comments on the manuscript. We thank Dr E. v. Kitzing for his assistance in deriving eqn (1). We would also like to thank S. Nestel, B. Joch, M. Winter, Dr C. Racca, C. Voigt and E. Dauer for technical assistance. This work was supported by the ‘von Helmholtz-Programm’ of the BMBF (J.L.) and the Minerva Foundation (H.M.).

Author's email address

H. Markram: bnmark@weizmann.weizmann.ac.il

Received 12 September 1996; accepted 10 December 1996.